IEEE Access
Multidisciplinary | Rapid Review | Open Access Journal

Received April 28, 2021, accepted May 14, 2021, date of publication May 17, 2021, date of current version May 26, 2021.

Digital Object Identifier 10.1109/ACCESS.2021.3081397

Time-Delayed Nonlinear Integral Resonant Controller to Eliminate the Nonlinear Oscillations of a Parametrically Excited System

N. A. SAEED[1], GALAL M. MOATIMID[2], FAWZY M. ELSABAA[2], YOMNA Y. ELLABBAN[2], S. K. ELAGAN[3], AND MOHAMED S. MOHAMED[3]

[1]Department of Physics and Engineering Mathematics, Faculty of Electronic Engineering, Menoufia University, Menouf 32952, Egypt
[2]Department of Mathematics, Faculty of Education, Ain Shams University, Cairo 11566, Egypt
[3]Department of Mathematics and Statistics, College of Science, Taif University, Taif 21944, Saudi Arabia

Corresponding author: N. A. Saeed (nasser.a.saeed@el-eng.menoufia.edu.eg)

This work was supported by the Taif University Researchers Supporting Project, Taif University, Taif, Saudi Arabia, under Grant TURSP-2020/160.

ABSTRACT In this work, a nonlinear integral resonant controller is utilized for the first time to suppress the principal parametric excitation of a nonlinear dynamical system. The whole system is modeled as a second-order nonlinear differential equation (i.e., main system) coupled to a nonlinear first-order differential equation (i.e., controller). The control loop time-delays are included in the studied model. The multiple scales homotopy approach is employed to obtain an approximate solution for the proposed time-delayed dynamical system. The nonlinear algebraic equation that governs the steady-state oscillation amplitude has been extracted. The effects of the time-delays, control gain, and feedback gains on the performance of the suggested controller have been investigated. The obtained results indicated that the controller performance depends on the product of the control and feedback signal gains as well as the sum of the time-delays in the control loop. Accordingly, two simple objective functions have been derived to design the optimum values of the loop-delays, control gain, and feedback gains in such a way that enhances the efficiency of the proposed controller. The analytical and numerical simulations illustrated that the proposed controller could eliminate the system vibrations effectively at specific values of the control and feedback signal gains. In addition, the selection method of the loop-delays that either enhances the control performance or destabilizes the system motion has been explained in detail.

INDEX TERMS Nonlinear integral resonant controller, parametric resonance, linear and nonlinear feedback control, time-delays, objective function, stability chart.

LIST OF SYMBOLS

$q_1, \dot{q}_1, \ddot{q}_1$	Displacement, velocity, and acceleration of the parametrically excited system.
$q_2, \dot{q}_2$	Displacement and velocity of the nonlinear resonant controller.
μ	Linear damping coefficients of the parametrically excited system
ω	Linear natural frequency of the parametrically excited system
α, β	Cubic nonlinearity coefficients of the parametrically excited system.
ηf	Excitation force amplitude of the parametrically excited system.
Ω	Excitation frequency of the parametrically excited system.
γ	The control signal gains.
δ_1, δ_2	The linear and nonlinear feedback signal gains.
λ	Feedback gain of the nonlinear resonant controller.
τ_1, τ_2	Time-delays of the closed loop.

The associate editor coordinating the review of this manuscript and approving it for publication was Agustin Leobardo Herrera-May.

I. INTRODUCTION

Excitation of nonlinear dynamical systems is called a parametric excitation when the excitation forces appear as coefficients of one or more variables in the governing equations

of motion. In most engineering applications, the nature of the excitation forces is periodic or can be considered periodic. The study of the time-periodic equations has found many engineering applications such as stability of the structures, nonlinear vibration control, dynamics of satellites, rotating machines, biomechanics…etc. In many situations, the mathematical models that govern the dynamical behaviors of such engineering systems are nonlinear differential equations with periodic coefficients. These types of differential equations are known as the parametrically excited systems. The nonlinear vibrations analysis and control of the parametrically excited systems were and still are the main subject of many research works, where Oueini and Nayfeh [1] investigated the principal parametric excitation control of a nonlinear cantilever beam system. As the nonlinear vibration amplitude of such systems cannot be fully controlled by the conventional control techniques such as adding linear damping using the ***linear-velocity*** feedback controller or connecting a conventional vibration absorber, the authors proposed the ***cubic-velocity*** feedback controller. The authors analyzed the system mathematical model utilizing the multiple time scales perturbations method. Depending on the obtained bifurcation diagrams and experimental validations, they concluded that the ***cubic-velocity*** feedback controller has higher efficiency than the ***linear-velocity*** controller in suppressing the principal parametric excitations of the considered system. Yabuno *et al.* [2] investigated the principal parametric oscillations of a cantilever beam system using a passive vibration absorber. The proposed absorber is a pendulum connected to the endpoint of a vertically suspended beam. Based on the obtained results, the authors concluded that the frictional force between the connected pendulum and the beam can mitigate the whole system's nonlinear vibrations. Chen [3] investigated the principal parametric vibration control of a vertically supported beam system. The author proposed three different versions of the active controllers, namely ***cubic-velocity, cubic-position***, and ***linear-velocity*** controllers. The obtained analytical and experimental results illustrated that the ***cubic-velocity*** feedback controller is the most efficient one. Pratiher [4] studied the nonlinear vibration control of a transversely excited cantilever beam system with a tip mass. The studied system is modeled as a parametrically excited nonlinear system. The author introduced the ***cubic-velocity*** controller to eliminate the principal parametric excitations, where the obtained results confirmed the efficiency of the suggested control method.

Time-delay is an essential issue in active vibration control techniques, where the existence of time-delay in the control loop may be the main reason for the system failure via destabilizing the control loop [5]–[17]. Accordingly, the influence of the time-delay on the performance of the different controllers has been discussed, where Macarri [5] explored the influence of the time-delays on the performance of a linear position-velocity feedback controller. Alhazza *et al.* [6] investigated the effect of the time-delay on the performance of a linear acceleration feedback controller utilized to mitigate the multimode oscillation of a cantilever beam system. Alhazza *et al.* [7] explored the effects of time-delays on the performance of the linear position, velocity, and acceleration controllers utilized to control the primary resonance vibrations of the cantilever beam system. Daqaq [8] discussed the effect of the time-delays on the performance of the linear and cubic versions of the position-velocity-acceleration feedback controller. Peng *et al.* [9] investigated the transversal nonlinear oscillations of a cantilever beam system at primary resonance utilizing the time-delayed linear position-velocity-acceleration controller. According to Refs. [6]–[9], The main conclusion is that the controlled system may lose its stability at specific values of the loop-delay. However, the time-delays can improve the controller efficiency in suppressing the system vibrations at other time-delays values. Saeed *et al.* [10]–[12] investigated the nonlinear vibration control of different dynamical systems applying the time-delayed linear and nonlinear position-velocity feedback controller. The authors derived a simple objective function to improve the performance of the controller at hand via selecting the optimal time-delays and control gains. Recently, Saeed *et al.* [13] have investigated the performance of six versions of the time-delayed linear and nonlinear position, velocity, and acceleration feedback controllers. The authors reported that the time-delayed cubic-acceleration controller is the most efficient one in both vibration mitigation and bifurcation suppression. Sun *et al.* introduced the time-delayed vibration isolators with multi-directional quasi-zero-stiffness [18]–[20]. The authors reported that the time-delayed control able to tune the isolators damping and stiffness coefficients, especially for the low-frequency range.

Linear and nonlinear forms of the Integral Resonant Controller (IRC) have been extensively introduced to suppress the nonlinear vibration of different nonlinear dynamical systems [21]–[26], where Diaz *et al.* [21] applied the IRC to control the nonlinear vibrations of the light-weight civil engineering structures. Al-Mamun *et al.* [22] utilized the nonlinear integral resonant controller to control the nonlinear oscillations of piezoelectric micro-actuator. Omidi and Mahmoodi [23], [24] introduced the nonlinear integral resonant controller in parallel to the positive position feedback controller. The authors reported that the IRC can enhance the positive position feedback controller efficiency via minimizing the resonant peaks. Omidi and Mahmoodi [25] proposed a modified version of the linear integral resonant controller known as the nonlinear integral resonant controller to control nonlinear smart structure oscillations. The authors concluded that the applied controller could suppress the system nonlinear vibration effectively. MacLean and Sumeet [26] applied the linear integral resonant control to the bifurcation behaviors of micro-cantilever beam structures. The authors concluded that the proposed control method can eliminate jump-phenomenon and hysteresis of the considered system via increasing the system linear damping coefficient.

Depending on the literature reviews, limited types of controllers have been succeeded in mitigating or eliminating

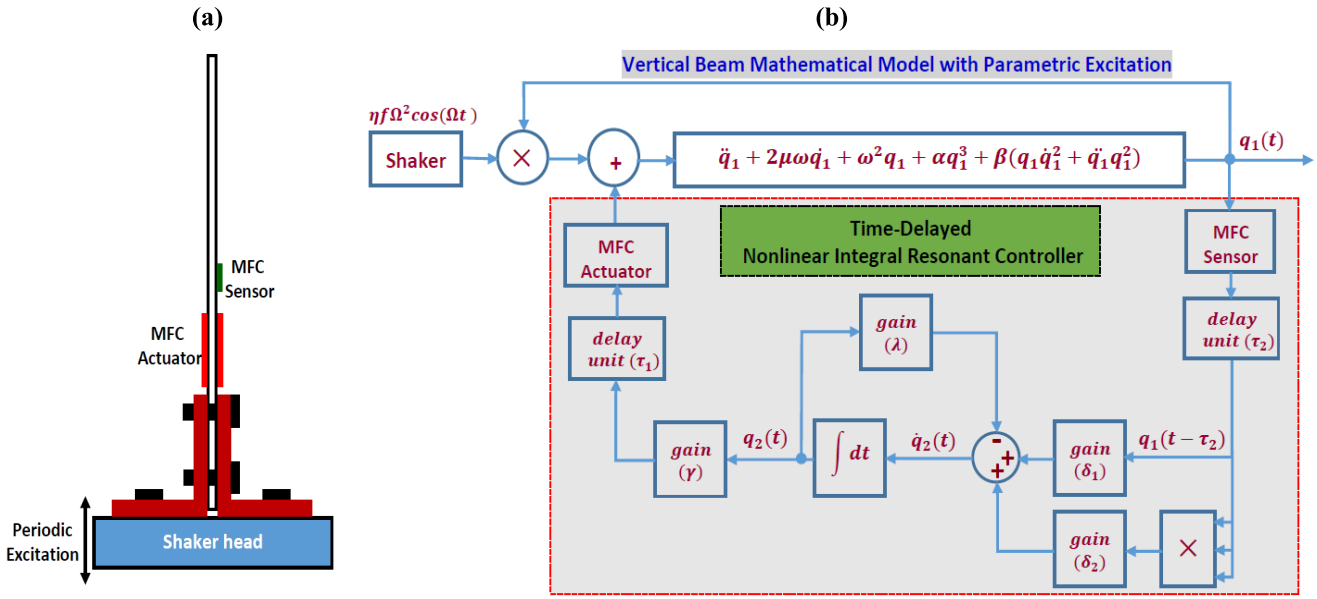

FIGURE 1. (a) Cantilever beam system under longitudinal excitation, and (b) The controlled system block diagram.

the nonlinear oscillations of the parametrically excited systems, effectively. These types are the cubic-velocity and cubic-acceleration feedback controllers [1], [3], [13]. In addition, the **N**onlinear **I**ntegral **R**esonant **C**ontroller (NIRC) never applied before to control the nonlinear oscillations of the parametrically excited systems. Accordingly, the NIRC is utilized within this work as a new control strategy to suppress the nonlinear oscillations of parametrically excitation cantilever beam system for the first time. The time delays in the control loop are included in the studied model. The slow flow modulating equations that govern the controlled system vibration amplitude are derived using the multiple scales homotopy approach. The obtained analytical results illustrated that the linear integral resonant controller could add linear damping to the controlled system that depends on the sum of the loop-delays and the product of the control gain and linear feedback gain. In addition, the nonlinear integral resonant controller adds nonlinear damping to the controlled system that depends on the sum of the loop-delays and the product of the control gain and nonlinear feedback gain. Accordingly, the obtained analytical results are validated numerically via plotting different response curves for the controlled system. The effects of the control gain, feedback gains, and loop delays on the system vibration amplitude are explored. The analytical and numerical simulations confirmed that the proposed control technique (i.e., NIRC) can suppress the vibration amplitude of the considered system to zero.

In comparing the current work with the previously published articles, it is the first time to apply a linear and nonlinear combination of the integral resonant controller to mitigate the nonlinear oscillation of a parametrically excited system. In addition, the effect of loop-delays has not been discussed before regarding the integral resonant controller [21]–[26]. Finally, the main contribution of this article is introducing the NIRC as a new and effective control strategy in suppressing the nonlinear oscillations of the parametrically excited systems besides the cubic-velocity and cubic-acceleration feedback controllers.

II. MATHEMATICAL MODEL AND SLOW FLOW MODULATING EQUATIONS

The nonlinear differential equation that governs the first-mode temporal oscillation of a parametrically excited cantilever beam system shown in Fig. 1a is given as follows (Ref. [27]):

$$\ddot{q}_1 + 2\mu\omega\dot{q}_1 + \omega^2 q_1 + \alpha q_1^3 + \beta(q_1\dot{q}_1^2 + \ddot{q}_1 q_1^2) = \eta q_1 f\Omega^2 \cos(\Omega t) + F_C \quad (1)$$

where F_c is the proposed control force. The Time-Delayed Nonlinear Integral Resonant Controller (TDNIRC) is introduced within this work to control the nonlinear oscillation of a parametrically excited system for the first time. Accordingly, the whole system mathematical model can be expressed as follows [25], [26]:

$$\ddot{q}_1 + 2\mu\omega\dot{q}_1 + \omega^2 q_1 + \alpha q_1^3 + \beta(q_1\dot{q}_1^2 + \ddot{q}_1 q_1^2) = \eta q_1 f\Omega^2 \cos(\Omega t) + \gamma q_2(t-\tau_1), \quad (2.1)$$

$$\dot{q}_2 + \lambda q_2 = \delta_1 q_1(t-\tau_2) + \delta_2 q_1^3(t-\tau_2). \quad (2.2)$$

where γ is the linear control gain, δ_1 is the linear feedback gain, δ_2 is the nonlinear feedback gain, and τ_1, τ_2 are the time-delays in the control loop as shown in Fig. 1b.

A. PRINCIPAL PARAMETRIC EXCITATIONS ($\Omega = 2\omega + \sigma$)

When the excitation frequency of a parametrically excited system is closed to twice its natural frequency (i.e., $\Omega = 2\omega$),

the excited system responds with high oscillation amplitude as a result of the principal parametric resonance occurrence. Within this work, the efficiency of the proposed controller (TDNIRC) in suppressing the principal parametric resonance of the considered system is investigated. Accordingly, the multiple scales homotopy technique is utilized to derive the slow flow modulating equations of the time-delayed nonlinear dynamical system given by Eqs. (2). Accordingly, the homotopy equation can be formulated as follows [28], [29]:

$$H(q_1, q_2, \rho) = L(q_1, q_2) + \rho N(q_1, q_2), \quad \rho \in [0, 1] \tag{3}$$

where $L(q_1, q_2)$ is the linear term of the given dynamical systems, $N(q_1, q_2)$ represents the nonlinear terms, and ρ is defined as the homotopy parameter. According to Eqs. (2) and (3), we can write the homotopy problem as follows:

$$\begin{aligned} &H_1(q_1, q_2, \rho) \\ &= \ddot{q}_1 + \omega^2 q_1 + \rho \left(2\mu\omega\dot{q}_1 + \alpha q_1^3 \right. \\ &\quad \left. + \beta(q_1\dot{q}_1^2 + \ddot{q}_1 q_1^2) - \eta q_1 f \Omega^2 \cos(\Omega t) - \gamma q_2(t - \tau_1)\right) \end{aligned} \tag{4.1}$$

$$\begin{aligned} &H_2(q_1, q_2, \rho) \\ &= \dot{q}_2 + \lambda q_2 - \delta_1 q_1(t - \tau_2) - \delta_2 q_1^3(t - \tau_2) \end{aligned} \tag{4.2}$$

Using the multiple time scales perturbations method [30], a two-time scale may be considered as follows:

$$q_1(t, \rho) = q_{10}(T_0, T_1) + \rho q_{11}(T_0, T_1) + O(\rho^2), \tag{5.1}$$

$$q_2(t, \rho) = q_{20}(T_0, T_1) + \rho q_{21}(T_0, T_1) + O(\rho^2). \tag{5.1}$$

$$\begin{aligned} q_1(t - \tau_2, \rho) &= q_{10}(T_0 - \tau_2, T_1 - \rho\tau_2) \\ &\quad + \rho q_{11}(T_0 - \tau_2, T_1 - \rho\tau_2) + O(\rho^2), \end{aligned} \tag{5.3}$$

$$\begin{aligned} q_2(t - \tau_1, \rho) &= q_{20}(T_0 - \tau_1, T_1 - \rho\tau_1) \\ &\quad + \rho q_{21}(T_0 - \tau_1, T_1 - \rho\tau_1) + O(\rho^2). \end{aligned} \tag{5.4}$$

where $T_0 = t$, and $T_1 = \rho t$. Accordingly, the time derivatives $\frac{d}{dt}$ and $\frac{d^2}{dt^2}$ can be expressed in terms of T_0 and T_1 as follows:

$$\begin{aligned} &\frac{d}{dt} = D_0 + \rho D_1, \quad \frac{d^2}{dt^2} = D_0^2 + 2\rho D_0 D_1, \\ &D_j = \frac{\partial}{\partial T_j}, \quad j = 0,\ 1 \end{aligned} \tag{6}$$

Substituting Eqs. (5) and (6) into Eqs. (4) with equating the coefficients of like power of the homotopy parameter ρ, we have:

$$\rho^0 : \left(D_0^2 + \omega^2\right) q_{10} = 0, \tag{7.1}$$

$$\begin{aligned} (D_0 + \lambda)\, q_{20} &= \delta_1 q_{10}(T_0 - \tau_2, T_1 - \tau_2) \\ &\quad + \delta_2 q_{10}^3(T_0 - \tau_2, T_1 - \tau_2). \end{aligned} \tag{7.2}$$

$$\begin{aligned} \rho^1 : \left(D_0^2 + \omega^2\right) q_{11} &= -2D_0 D_1 q_{10} - 2\mu\omega D_0 q_{10} - \alpha q_{10}^3 \\ &\quad - \beta q_{10}(D_0 q_{10})^2 - \beta q_{10}^2 D_0^2 q_{10} \\ &\quad + \eta q_{10}\Omega^2 f \cos(\Omega T_0) \\ &\quad + \gamma q_{20}(T_0 - \tau_1, T_1 - \tau_1) \end{aligned} \tag{8.1}$$

$$\begin{aligned} (D_0 + \lambda)\, q_{21} &= -D_1 q_{20} + \delta_1 q_{11}(T_0 - \tau_2, T_1 - \tau_2) \\ &\quad + 3\delta_2 q_{10}^2(T_0 - \tau_2, T_1 - \tau_2) \\ &\quad \times q_{11}(T_0 - \tau_2, T_1 - \tau_2) \end{aligned} \tag{8.2}$$

The solution of Eqs. (7) can be expressed as follows:

$$q_{10}(T_0, T_1) = A(T_1)e^{i\omega T_0} + cc \tag{9.1}$$

$$\begin{aligned} q_{20}(T_0, T_1) &= \frac{\delta_2(\lambda - 3i\omega)}{(\lambda^2 + 9\omega^2)} A^3 e^{3i\omega(T_0 - \tau_2)} \\ &\quad + \frac{(\lambda - i\omega)}{(\lambda^2 + \omega^2)}(A\delta_1 + 3A^2\bar{A}\delta_2)e^{i\omega(T_0 - \tau_2)} \\ &\quad + C(T_1)e^{-\lambda T_0} + cc \end{aligned} \tag{9.2}$$

where cc denotes the complex conjugate terms. According to Eqs. (9.2), the time-delayed solution can be expressed as follows:

$$\begin{aligned} q_{20}(T_0 - \tau_1, T_1) &= \frac{\delta_2(\lambda - 3i\omega)}{(\lambda^2 + 9\omega^2)} A^3 e^{3i\omega(T_0 - \tau_1 - \tau_2)} \\ &\quad + \frac{(\lambda - i\omega)}{(\lambda^2 + \omega^2)}(A\delta_1 + 3A^2\bar{A}\delta_2)e^{i\omega(T_0 - \tau_1 - \tau_2)} \\ &\quad + C(T_1)e^{-\lambda(T_0 - \tau_1)} + cc \end{aligned} \tag{10}$$

Substituting Eqs. (9) and (10) into Eq. (8.1), we have

$$\begin{aligned} \left(D_0^2 + \omega^2\right) q_{11} &= e^{i\omega T_0}\left(-2\, i\omega D_1 A + A\,(-2\, i\mu\omega^2 \right. \\ &\quad \left. + \frac{\gamma\delta_1(\lambda - i\omega)}{(\lambda^2 + \omega^2)}\, e^{-i\omega(\tau_1 + \tau_2)}\right) \\ &\quad + A^2\bar{A}\left(-3\,\alpha + 2\beta\omega^2 \right. \\ &\quad \left. + \frac{3\gamma\delta_2(\lambda - i\omega)}{(\lambda^2 + \omega^2)}\, e^{-i\omega(\tau_1 + \tau_2)}\right) \\ &\quad + \frac{\eta f}{2}(2\omega + \sigma)^2\bar{A}\, e^{i\sigma T_1}\Big) \\ &\quad + (A^3(-\alpha + 2\omega^2\beta \\ &\quad + \frac{\gamma\delta_2(\lambda - 3i\omega)}{(\lambda^2 + 9\omega^2)}e^{-3i\omega(\tau_1 + \tau_2)}) \\ &\quad + \frac{\eta f}{2}(2\omega + \sigma)^2 A e^{i\sigma T_1})e^{3i\omega T_0} \\ &\quad + \gamma C(T_1)e^{-\lambda(T_0 - \tau_1)} + cc \end{aligned} \tag{11}$$

After forcing the secular term in Eq. (11) to be zero, the equation solution can be expressed as follows:

$$q_{11}(T_0,T_1) = -\frac{1}{8\omega^2}(A^3(-\alpha+2\omega^2\beta + \frac{\gamma\delta_2(\lambda-3i\omega)}{(\lambda^2+9\omega^2)}e^{-3i(\omega\tau_1+\tau_2)}) + \frac{\eta f}{2}(2\omega+\sigma)^2 A e^{i\sigma T_1})e^{3i\omega T_0} + \frac{\gamma}{(\omega^2+\lambda^2)}C(T_1)e^{-\lambda(T_0-\tau_1)} + cc \quad (12)$$

According to Eq. (12), the time-delayed solution can be expressed as follows:

$$q_{11}(T_0-\tau_2,T_1) = -\frac{1}{8\omega^2}(A^3(-\alpha+2\omega^2\beta + \frac{\gamma\delta_2(\lambda-3i\omega)}{(\lambda^2+9\omega^2)}e^{-3i(\omega\tau_1+\tau_2)}) + \frac{\eta f}{2}(2\omega+\sigma)^2 A e^{i\sigma T_1})e^{3i\omega(T_0-\tau_2)} + \frac{\gamma}{(\omega^2+\lambda^2)}C(T_1)e^{-\lambda(T_0-\tau_1-\tau_2)} + cc \quad (13)$$

Based on Eqs. (9) and (12), one can find the solvability condition of Eq. (8.2) as follows:

$$(D_1+M)\,C(T_1) = 0 \quad (14)$$

According to Eq. (14), we have

$$C(T_1) = \psi e^{-\int M dT_1}, \quad \psi = constant,$$
$$M = -(\delta_1 + 6\delta_2 A\bar{A})\frac{\gamma e^{\lambda(\tau_1+\tau_2)}}{(\omega^2+\lambda^2)} \quad (15)$$

Accordingly, the solvability condition of Eq. (11) can be given as:

$$-2i\omega D_1 A + A\left(-2\,i\mu\omega^2 + \frac{\gamma\delta_1(\lambda-i\omega)}{(\lambda^2+\omega^2)}\,e^{-i\omega(\tau_1+\tau_2)}\right) + A^2\bar{A}\left(-3\,\alpha+2\beta\omega^2 + \frac{3\gamma\delta_2(\lambda-i\omega)}{(\lambda^2+\omega^2)}\,e^{-i\omega(\tau_1+\tau_2)}\right) + \frac{\eta f}{2}(2\omega+\sigma)^2\bar{A}e^{i\sigma T_1} = 0 \quad (16)$$

Multiplying Eq. (16) by ρ with making ρ tends to unity and by using Eq. (6), we have

$$-2i\omega\frac{dA}{dt} + A\left(-2\,i\mu\omega^2 + \frac{\gamma\delta_1(\lambda-i\omega)}{(\lambda^2+\omega^2)}\,e^{-i\omega(\tau_1+\tau_2)}\right) + A^2\bar{A}\left(-3\,\alpha+2\beta\omega^2 + \frac{3\gamma\delta_2(\lambda-i\omega)}{(\lambda^2+\omega^2)}\,e^{-i\omega(\tau_1+\tau_2)}\right) + \frac{\eta f}{2}(2\omega+\sigma)^2\bar{A}e^{i\sigma t} = 0 \quad (17)$$

Equation (17) is a first-order nonlinear differential equation with complex coefficients. Following Nayfeh and Mook [30], the function $A(t)$ may be expressed in a polar form as:

$$A(t) = \frac{1}{2}a(t)e^{i\theta(t)} \quad (18)$$

where $a(t)$ is the instantaneous oscillation amplitude of the periodically excited system given by Eqs. (2), and $\theta(t)$ is the corresponding phase-angle. Inserting Eq. (18) into Eq. (17)

$$-i\omega(\dot{a}+i\dot{\theta}a)e^{i\theta} + \frac{1}{2}a\left(-2\,i\mu\omega^2 + \frac{\gamma\delta_1(\lambda-i\omega)}{(\lambda^2+\omega^2)} \times e^{-i\omega(\tau_1+\tau_2)}\right)e^{i\theta} + \frac{1}{8}a^3\left(-3\,\alpha+2\beta\omega^2 + \frac{3\gamma\delta_2(\lambda-i\omega)}{(\lambda^2+\omega^2)} \times e^{-i\omega(\tau_1+\tau_2)}\right)e^{i\theta} + \frac{\eta f}{4}a(2\omega+\sigma)^2 e^{i(\sigma t-\theta)} = 0 \quad (19)$$

Dividing Eq. (19) by $e^{i\theta}$, and let $\phi = \sigma t - 2\theta$, yields:

$$-i\omega(\dot{a}+i\dot{\theta}a) + \frac{1}{2}a\left(-2\,i\mu\omega^2 + \frac{\gamma\delta_1(\lambda-i\omega)}{(\lambda^2+\omega^2)}\,e^{-i\omega(\tau_1+\tau_2)}\right) + \frac{1}{8}a^3\left(-3\,\alpha+2\beta\omega^2 + \frac{3\gamma\delta_2(\lambda-i\omega)}{(\lambda^2+\omega^2)}\,e^{-i\omega(\tau_1+\tau_2)}\right)e^{i\theta} + \frac{\eta f}{4}a(2\omega+\sigma)^2 e^{i\varphi} = 0 \quad (20)$$

Expanding Eq. (20) to separate the real and imaginary part [31], we have:

$$-\dot{\phi} + \left(\sigma - \frac{\gamma\delta_1}{(\omega^2+\lambda^2)}\sin(\omega\tau_1+\omega\tau_2) + \frac{\lambda\gamma\delta_1}{\omega(\omega^2+\lambda^2)}\cos(\omega\tau_1+\omega\tau_2)\right) + \frac{a^2}{4\omega}(-3\,\alpha + 2\omega^2\beta - \frac{3\omega\gamma\delta_2}{(\omega^2+\lambda^2)}\sin(\omega\tau_1+\omega\tau_2) + \frac{3\lambda\gamma\delta_2}{(\omega^2+\lambda^2)} \times \cos(\omega\tau_1+\omega\tau_2)) + \frac{\eta f}{2\omega}(2\omega+\sigma)^2\cos(\phi) + i\left(-\dot{a} - \omega a\left(\mu + \frac{\lambda\gamma\delta_1}{2\omega^2(\omega^2+\lambda^2)}\sin(\omega\tau_1+\omega\tau_2) + \frac{\gamma\delta_1}{2\omega(\omega^2+\lambda^2)}\cos(\omega\tau_1+\omega\tau_2)\right) - \omega^3 a^3 \times \left(\frac{3\lambda\gamma\delta_2}{8\omega^4(\omega^2+\lambda^2)}\sin(\omega\tau_1+\omega\tau_2) + \frac{3\gamma\delta_2}{8\omega^3(\omega^2+\lambda^2)}\cos(\omega\tau_1+\omega\tau_2)\right) + \frac{\eta f a}{4\omega}(2\omega+\sigma)^2\sin(\phi)\right) = 0 \quad (21)$$

Separating the real and imaginary part of Eq. (21), we get:

$$\dot{a} = -\omega a\left(\mu + \frac{\lambda\gamma\delta_1}{2\omega^2(\omega^2+\lambda^2)}\sin(\omega\tau_1+\omega\tau_2) + \frac{\gamma\delta_1}{2\omega(\omega^2+\lambda^2)}\cos(\omega\tau_1+\omega\tau_2)\right) - \omega^3 a^3\left(\frac{3\lambda\gamma\delta_2}{8\omega^4(\omega^2+\lambda^2)}\sin(\omega\tau_1+\omega\tau_2) + \frac{3\gamma\delta_2}{8\omega^3(\omega^2+\lambda^2)}\cos(\omega\tau_1+\omega\tau_2)\right) + \frac{\eta f a}{4\omega}(2\omega+\sigma)^2\sin(\phi), \quad (22.1)$$

$$\dot{\phi} = \left(\sigma - \frac{\gamma\delta_1}{(\omega^2+\lambda^2)}\sin(\omega\tau_1+\omega\tau_2)\right.$$

$$+\frac{\lambda\gamma\delta_1}{\omega(\omega^2+\lambda^2)}\cos(\omega\tau_1+\omega\tau_2)\Big)$$
$$+\frac{a^2}{4\omega}\left(-3\,\alpha+2\omega^2\beta-\frac{3\omega\gamma\delta_2}{(\omega^2+\lambda^2)}\sin(\omega\tau_1+\omega\tau_2)\right.$$
$$\left.+\frac{3\lambda\gamma\delta_2}{(\omega^2+\lambda^2)}\cos(\omega\tau_1+\omega\tau_2)\right)$$
$$+\frac{\eta f}{2\omega}(2\omega+\sigma)^2\cos(\phi). \tag{22.2}$$

Eqs. (22) are the slow flow modulating equations that govern the evaluations of both the oscillation amplitude and the phase angle of the periodically excited system given by Eqs. (2). At steady-state oscillations, the rate of change of the oscillation amplitude and phase angle is zero, which means that $\dot{a}=\dot{\phi}=0.0$. Substituting $\dot{a}=\dot{\phi}=0.0$ into Eqs. (22), we have

$$\frac{\eta f a}{4\omega}(2\omega+\sigma)^2\sin(\phi)$$
$$=\omega a\left(\mu+\frac{\lambda\gamma\delta_1}{2\omega^2(\omega^2+\lambda^2)}\right.$$
$$\left.\times\sin(\omega\tau_1+\omega\tau_2)+\frac{\gamma\delta_1}{2\omega(\omega^2+\lambda^2)}\cos(\omega\tau_1+\omega\tau_2)\right)$$
$$+\omega^3a^3\left(\frac{3\lambda\gamma\delta_2}{8\omega^4(\omega^2+\lambda^2)}\sin(\omega\tau_1+\omega\tau_2)\right.$$
$$\left.+\frac{3\gamma\delta_2}{8\omega^3(\omega^2+\lambda^2)}\cos(\omega\tau_1+\omega\tau_2)\right), \tag{23.1}$$
$$-\frac{\eta f}{2\omega}(2\omega+\sigma)^2\cos(\phi)$$
$$=\left(\sigma-\frac{\gamma\delta_1}{(\omega^2+\lambda^2)}\right.$$
$$\left.\times\sin(\omega\tau_1+\omega\tau_2)+\frac{\lambda\gamma\delta_1}{\omega(\omega^2+\lambda^2)}\cos(\omega\tau_1+\omega\tau_2)\right)$$
$$+\frac{a^2}{4\omega}\left(-3\alpha+2\omega^2\beta-\frac{3\omega\gamma\delta_2}{(\omega^2+\lambda^2)}\sin(\omega\tau_1+\omega\tau_2)\right.$$
$$\left.+\frac{3\lambda\gamma\delta_2}{(\omega^2+\lambda^2)}\cos(\omega\tau_1+\omega\tau_2)\right). \tag{23.2}$$

By squaring and adding Eqs. (23), we can obtain the following nonlinear algebraic equation:

$$\frac{\eta^2f^2}{4\omega^2}(2\omega+\sigma)^4$$
$$=\left[-2\omega\left(\mu+\frac{\lambda\gamma\delta_1}{2\omega^2(\omega^2+\lambda^2)}\right.\right.$$
$$\left.\times\sin(\omega\tau_1+\omega\tau_2)+\frac{\gamma\delta_1}{2\omega(\omega^2+\lambda^2)}\cos(\omega\tau_1+\omega\tau_2)\right)$$
$$-\frac{3a^2}{4}\left(\frac{\lambda\gamma\delta_2}{\omega(\omega^2+\lambda^2)}\sin(\omega\tau_1+\omega\tau_2)\right.$$
$$\left.\left.+\frac{\gamma\delta_2}{(\omega^2+\lambda^2)}\cos(\omega\tau_1+\omega\tau_2)\right)\right]^2$$
$$+\left[\left(\sigma-\frac{\gamma\delta_1}{(\omega^2+\lambda^2)}\sin\omega(\tau_1+\tau_2)+\right.\right.$$
$$\left.+\frac{\lambda\gamma\delta_1}{\omega(\omega^2+\lambda^2)}\cos\omega(\tau_1+\tau_2)\right)+\frac{a^2}{4\omega}(-3\,\alpha$$
$$+2\omega^2\beta-\frac{3\omega\gamma\delta_2}{(\omega^2+\lambda^2)}\sin(\omega\tau_1+\omega\tau_2)$$
$$\left.+\frac{3\lambda\gamma\delta_2}{(\omega^2+\lambda^2)}\cos(\omega\tau_1+\omega\tau_2))\right]^2 \tag{24}$$

Equation (24) is known as the frequency response equation that governs the steady-state oscillation amplitude of Eq. (2) as a function of the different system parameters (i.e., μ,α,β,η,f) and control parameters (i.e., $\gamma,\delta_1,\delta_2,\lambda,\tau_1,\tau_2$). Accordingly, the influence of the different control parameters (i.e., $\gamma,\delta_1,\delta_2,\tau_1,\tau_2$) on the main system oscillation amplitude (i.e., a) can be explored via solving Eq. (24) as illustrated in the next section. Moreover, to investigate the solution stability of Eq. (24), the Lyapunov direct method can be applied via examining the eigenvalues of the Jacobian matrix of the dynamical system given by Eqs. (22). Let a_{10} and ϕ_{10} is the solution of Eqs. (24), and a_{11} and ϕ_{11} are a small perturbation about this solution, we can assume

$$a=a_{10}+a_{11},\quad \phi=\phi_{10}+\phi_{11}\Rightarrow\dot{a}=\dot{a}_{11},\ \dot{\phi}=\dot{\phi}_{11}. \tag{25}$$

By substituting Eq. (25) into Eqs. (22), and expanding the resulting equations for the small perturbation, and keeping only the linear terms, one can obtain the following linear dynamical system:

$$\begin{pmatrix}\dot{a}_{11}\\ \dot{\phi}_{11}\end{pmatrix}=\begin{pmatrix}J_{11}&J_{12}\\ J_{21}&J_{22}\end{pmatrix}\quad\begin{pmatrix}a_{11}\\ \phi_{11}\end{pmatrix} \tag{26}$$

The above square matrix is the Jacobian matrix of the nonlinear system given by Eq. (22), where

$$J_{11}=-\omega\left(\mu+\frac{\lambda\gamma\delta_1}{2\omega^2(\omega^2+\lambda^2)}\sin(\omega\tau_1+\omega\tau_2)\right.$$
$$\left.+\frac{\gamma\delta_1}{2\omega(\omega^2+\lambda^2)}\cos(\omega\tau_1+\omega\tau_2)\right)$$
$$-\frac{9a^2}{8}\left(\frac{\lambda\gamma\delta_2}{\omega(\omega^2+\lambda^2)}\sin(\omega\tau_1+\omega\tau_2)\right.$$
$$\left.+\frac{\gamma\delta_2}{(\omega^2+\lambda^2)}\cos(\omega\tau_1+\omega\tau_2)\right)+\frac{\eta f}{4\omega}(2\omega+\sigma)^2\sin(\phi),$$
$$J_{12}=\frac{\eta f a}{4\omega}(2\omega+\sigma)^2\cos(\phi),$$
$$J_{21}=\frac{a}{2\omega}\left(-3\,\alpha+2\omega^2\beta-\frac{3\omega\gamma\delta_2}{(\omega^2+\lambda^2)}\sin(\omega\tau_1+\omega\tau_2)\right.$$
$$\left.+\frac{3\lambda\gamma\delta_2}{(\omega^2+\lambda^2)}\cos(\omega\tau_1+\omega\tau_2)\right),$$
$$J_{22}=-\frac{\eta f}{2\omega}(2\omega+\sigma)^2\sin(\phi).$$

According to the above Jacobin matrix, the characteristic polynomial of the linear system given by Eq. (26) is:

$$\Delta^2-(J_{11}+J_{22})\Delta+(J_{11}J_{22}-J_{12}J_{21})=0 \tag{27}$$

where the necessary and sufficient conditions for the stability of Eq. (24) may be expressed as follows depending on the Routh-Hurwitz criterion:

$$J_{11}+J_{22}<0\quad\text{and}\ J_{11}J_{22}-J_{12}J_{21}>0 \tag{28}$$

Accordingly, the efficiency of the applied controller (i.e., TDNIRC) in suppressing the nonlinear vibration of the considered system (i.e., cantilever beam system) can be explored via plotting the system vibration oscillation amplitude (a) against the detuning parameter (σ) at the different values of the controller parameters (i.e., $\gamma, \delta_1, \delta_2, \tau_1, \tau_2$) using Eq. (24). In addition, the stability behaviors can be investigated by applying the conditions given by Eq. (28).

III. RESPONSE CURVES AND TEMPORAL OSCILLATIONS

The efficiency of the proposed controller (TDNIRC) in eliminating the nonlinear principal parametric oscillations of the cantilever beam system is investigated within this section. The system vibration amplitude (a) is plotted versus the detuning parameter (σ) for the different values of the control parameters ($\gamma, \delta_1, \delta_2, \tau_1, \tau_2$) via solving Eq. (24). In addition, the stability of the obtained solution has been checked according to the Routh-Hurwitz criterion using Eq. (28). The stable solutions are plotted as a solid line while the unstable solutions are plotted as dashed ones. Moreover, the controlled system temporal equations (i.e., Eqs. (2)) have been solved numerically using MATLAB algorithms **ODE45** (when $\tau_1 = \tau_2 = 0.0$) and **DDE23** (when $\tau_1 \neq 0.0, \tau_2 \neq 0.0$) to confirm the obtained analytical results. The analytical and numerical simulations are performed utilizing the following values of the system parameters [27]: $f = 0.1, \eta = 1.5, \mu = 0.05, \omega = 3.06, \alpha = 14.4, \beta = 3.27, \Omega = 2\omega + \sigma, \lambda = 1.0, \gamma = 1.0, \delta_1 = 1.0, \delta_2 = 1.0$, and $\tau_1 = \tau_2 = 0.0$, unless otherwise mentioned.

A. SYSTEM OSCILLATORY BEHAVIOR BEFORE CONTROL

The main system frequency-response and force-response curves before control are illustrated in Fig. 2, where Fig. 2a shows the system frequency-response curve when the excitation force $f = 0.1$, and Fig. 2b illustrates the system force-response curve for three different values of the detuning parameter σ. It is clear from Fig. 2a that the parametrically excited system can exhibit a jump phenomenon either when increasing or decreasing the excitation frequency (Ω) about twice of its natural frequency (2ω). Increasing σ (i.e., increasing $\Omega = 2\omega + \sigma$) from the negative to the positive values, the system vibration amplitude will follow the path AB with the trivial solution (i.e., $a = 0$) until σ reaches the point B. For a very slight increase of σ beyond the point B, an abrupt increase of the oscillation amplitude will occur (jump from B to C) where the system oscillation amplitude will follow the path CDE. On the other hand, decreasing σ from the positive to the negative values, the system vibration amplitude will follow the path EDC until it reaches the point F. For a very slight decrease of σ beyond this value, an abrupt decrease of the oscillation amplitude will occur where the system amplitude will jump down from the point F to A. By examining Fig. 2a, we can confirm that the parametrically excited system may respond with a single nontrivial stable solution when σ lies between the points A and B, while if σ lies on the right hand of the point B, the system will exhibit a trivial oscillation amplitude. Besides, if σ lies between the points A and B, the system will perform one of two stable solutions depending on the initial conditions, where one of them is the trivial solution. Moreover, Fig. 2b shows that the vibration amplitude (a) is a monotonic increasing function of the excitation force regardless of the detuning parameters. The main objective of the current study is to control these dynamical behaviors and to eliminate the nonlinear oscillations of such systems. Accordingly, a novel control method (i.e., TDNIRC) is introduced within this work for the first time to investigate its efficiency in controlling dynamical behaviors of the parametrically excited nonlinear systems as explained in sections III.B and III.C.

B. THE NONLINEAR INTEGRAL RESONANT CONTROLLER WHEN $\tau_1 = \tau_2 = 0.0$

The performance of the Nonlinear Integral Resonant Controller (NIRC) in eliminating the nonlinear vibration of the system principal parametric excitations (when the time delay is zero) is explored within this subsection. The dynamical behaviors of the applied controller can be explained simply depending on the obtained slow flow modulating equations (i.e., Eqs. (22)) when $\tau_1 = \tau_2 = 0.0$. It is clear from Eq. 22a that the applied controller has modified the system linear damping coefficient (μ_L) and nonlinear damping coefficient (μ_N) to become:

$$\left.\begin{aligned} \mu_L(\gamma, \delta_1) &= \mu + \frac{\gamma\delta_1}{2\omega(\omega^2 + \lambda^2)}, \\ \mu_N(\gamma, \delta_2) &= \frac{3\gamma\delta_2}{8\omega^3(\omega^2 + \lambda^2)} \end{aligned}\right\} \tag{29}$$

It is clear from Eq. (25) that the linear damping coefficient (μ_L) depends on the product of both the control signal gain (γ) and the linear feedback signal gain (δ_1), while the nonlinear damping coefficient (μ_N) depends on the product of both the control signal gain (γ) and the nonlinear feedback signal gain (δ_2). Accordingly, $\mu_L\mu_N$ are plotted as two-variable functions as shown in Fig. 3.

In the light of the above explanations, the controlled system frequency-response curve is plotted via solving Eq. (24) for the different values of both the control and feedback signal gains as illustrated in Figs. 4 to 8. The efficiency of the Linear Integral Resonant Controller (LIRC) is explored through Figs. 4 and 5, where Fig.4a illustrates the system frequency-response curve for four different values of the control signal gain ($\gamma = 1, 2, 4, 6$) when $\delta_1 = 1.0$ and $\delta_2 = 0.0$, while Fig. 4b shows the system frequency-response curve for four different values of the linear feedback signal gain (i.e. $\delta_1 = 1, 2, 4, 6$) when $\gamma = 1.0$ and $\delta_2 = 0.0$. In general, Fig. 4 confirms that the effect of increasing either γ or δ_1 on the system oscillation amplitude is the same because the equivalent linear damping coefficient (μ_L) depends on the product of γ and δ_1 as in Eq. (29). In addition, the figure illustrates that the increasing of γ or δ_1, decreases the system oscillations amplitudes due to increasing the system equivalent linear damping coefficient (μ_L).

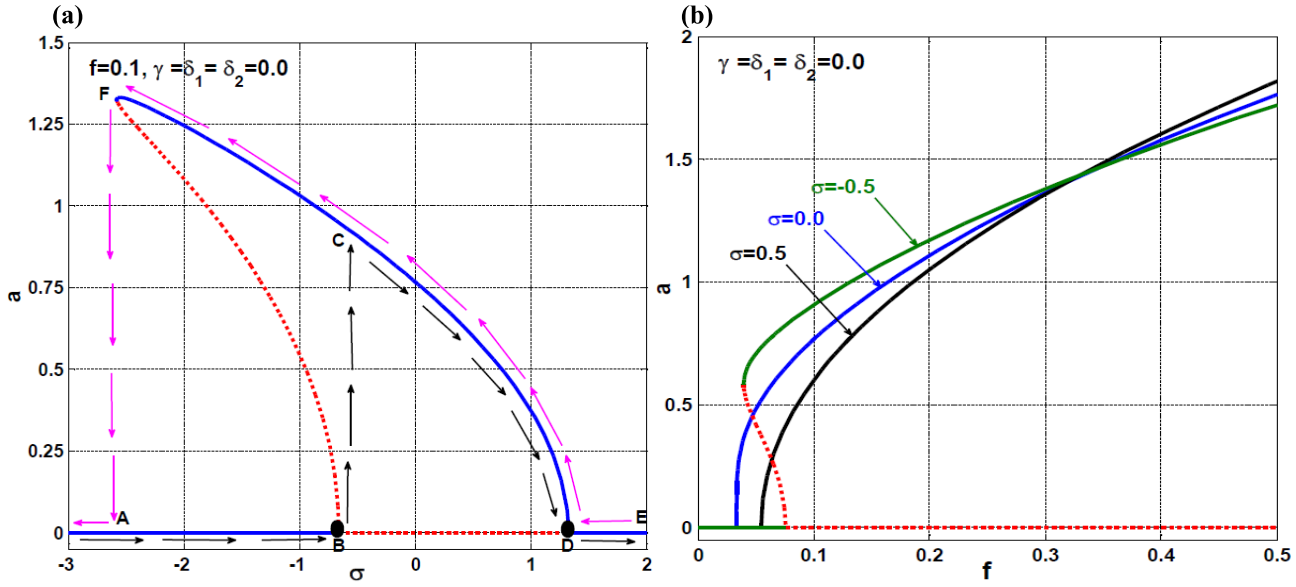

FIGURE 2. The system response curves before control: (a) frequency-response curve when $f = 0.1$, and (b) force-response curves when $\sigma = -0.5, 0.0,$ and 0.5.

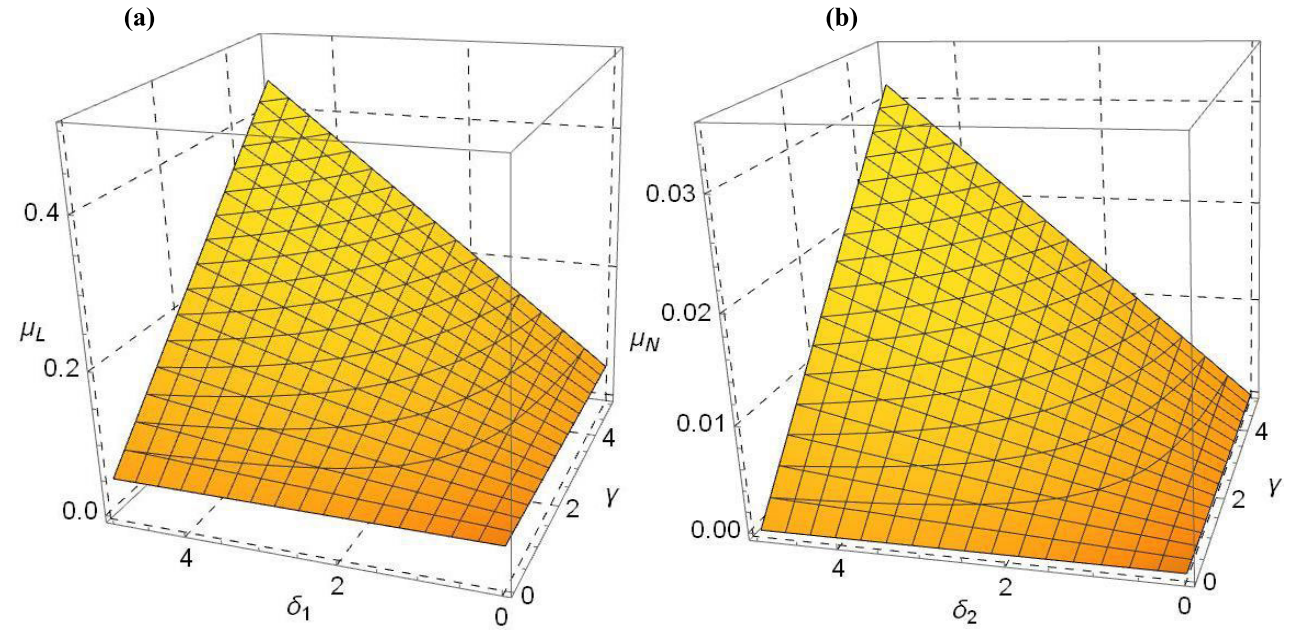

FIGURE 3. The controlled system equivalent damping coefficients μ_L and μ_N as a function of the control gain γ and feedback gains δ_1 and δ_2: (a) the equivalent linear damping coefficient μ_L as a function of the control gain γ and feedback gain δ_1, and (b) the equivalent nonlinear damping coefficient μ_N as a function of the control gain γ and feedback gain δ_2.

It is well known that Figs. 3 and 4 are obtained based on Eq. (24) that represents the approximate solution of the original dynamical system given by Eqs. (2). Accordingly, to confirm the accuracy of the obtained frequency-response curves given in Fig. 4, Eqs. (2) have been solved numerically using the MATLAB ODE45 algorithm, where the system temporal oscillation is simulated as shown in Fig. 5. Fig. 5a illustrates the controlled system temporal oscillation according to Fig. 4a when $f = 0.1, \sigma = 0.0, \delta_1 = 1.0, \delta_2 = 0.0$ for three different values of the control signal gain (i.e. $\gamma = 2, 4, 6$), while Fig. 5b shows the controlled system temporal oscillation according to Fig. 4b when $f = 0.1, \sigma = 0.0, \gamma = 1.0, \delta_2 = 0.0$ for three different values of the linear feedback signal gain (i.e. $\delta_1 = 2, 4, 6$). By examining Fig. 5, we can deduce that the considered system vibration amplitude is a monotonic decreasing function of both the control signal gain (γ) and the linear feedback signal gain (δ_1). Moreover, Fig. 5 confirms the excellent agreement of the numerical simulations with the analytical results that are given by Fig. 4.

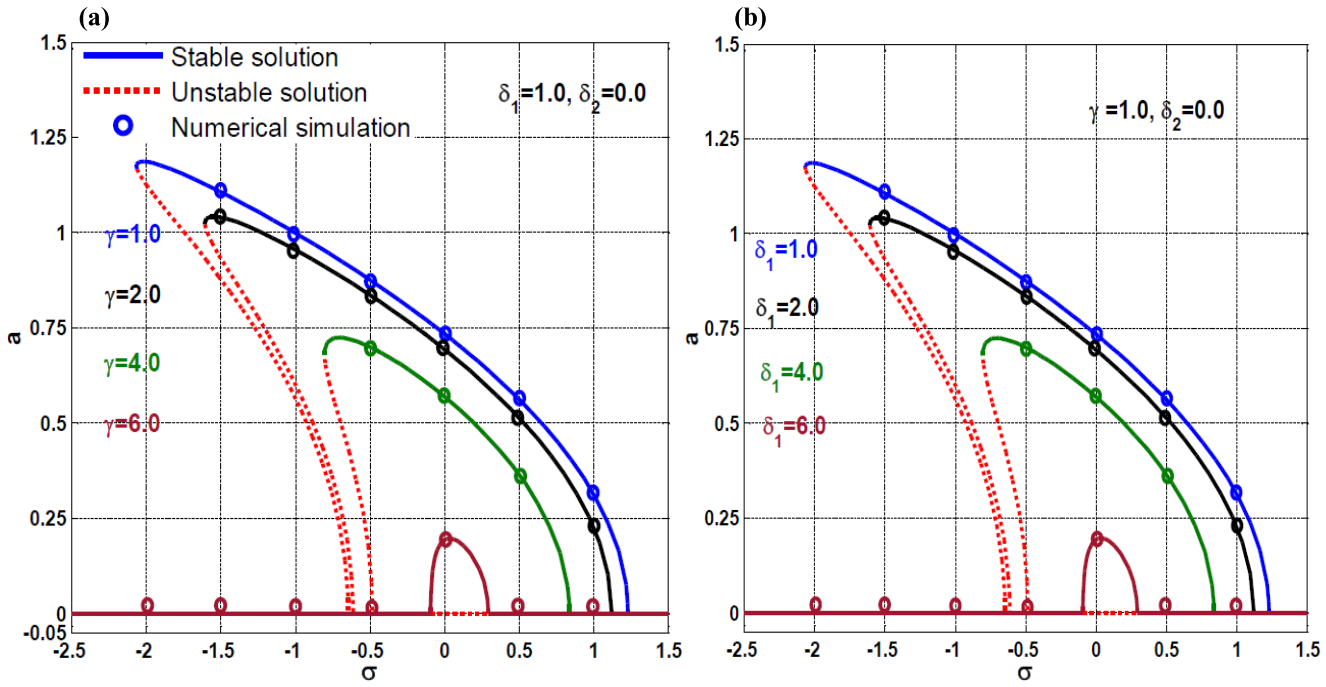

FIGURE 4. The controlled system frequency-response curves at different values of both the linear control and feedback gains when $\delta_2 = 0.0$: (a) the system frequency-response curve at four different values of the control signal gain γ when $\delta_1 = 1.0$, and (b) the system frequency-response curve at four different values of the linear feedback signal gain δ_1 when $\gamma = 1.0$.

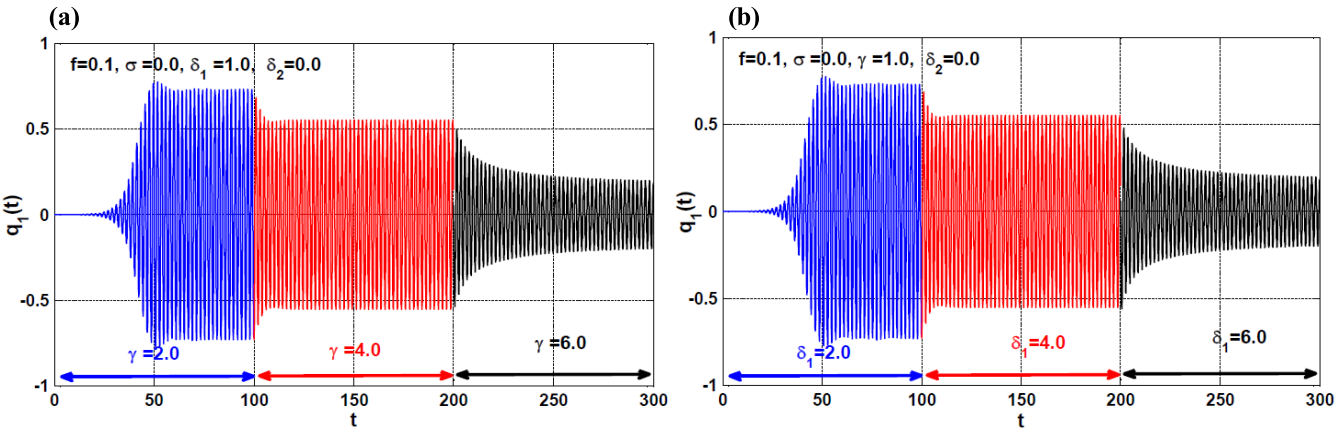

FIGURE 5. The time-history of the controlled system at $\sigma = 0$ according to Fig. 4: (a) the system time history when sweeping the control gain (γ) from 2 to 4, then to 6, and (b) the system time history when sweeping the linear feedback gain (δ_1) from 2 to 4, then to 6.

According to Eq. (29), the nonlinear damping coefficient (μ_N) is proportional to the product of both the control signal gain (γ) and the nonlinear feedback signal gain (δ_2). Accordingly, the controlled system frequency-response curve when $\delta_1 = 0.0$ is illustrated in Fig. 6. Fig. 6a shows the system frequency-response curve of the considered system when $\gamma = 1.0, \delta_1 = 0.0$ for four different values of the nonlinear feedback signal gain (i.e., $\delta_2 = 1, 2, 4, 6$), while Fig. 6b illustrates the controlled system frequency-response curve at $\delta_1 = 0.0$ for four different values of the linear control gain and nonlinear feedback gain (i.e, $\gamma = \delta_2 = 1, 2, 4, 6$). Comparing Figs. 6a and 6.b, we can deduce that the system vibration amplitude is a monotonic decreasing function of the product of the linear control gain (γ) and the nonlinear feedback gain (δ_2).

The efficiency of both the LIRC and NIRC are compared as shown in Fig. 7, where Fig. 7a shows the considered system frequency-response curve when $\delta_2 = 0.0$ for three different values of $\gamma = \delta_1 = 1, 2, 3$ and Fig. 7b illustrates the same frequency-response curve for three different values of $\gamma = \delta_1 = \delta_2 = 1, 2, 3$. Comparing Fig. 7a and 7b, we can deduce that two controllers have eliminated the system vibration at $\gamma = \delta_1 = \delta_2 = 3$. However, the NIRC has the highest efficiency in mitigating the system vibrations when

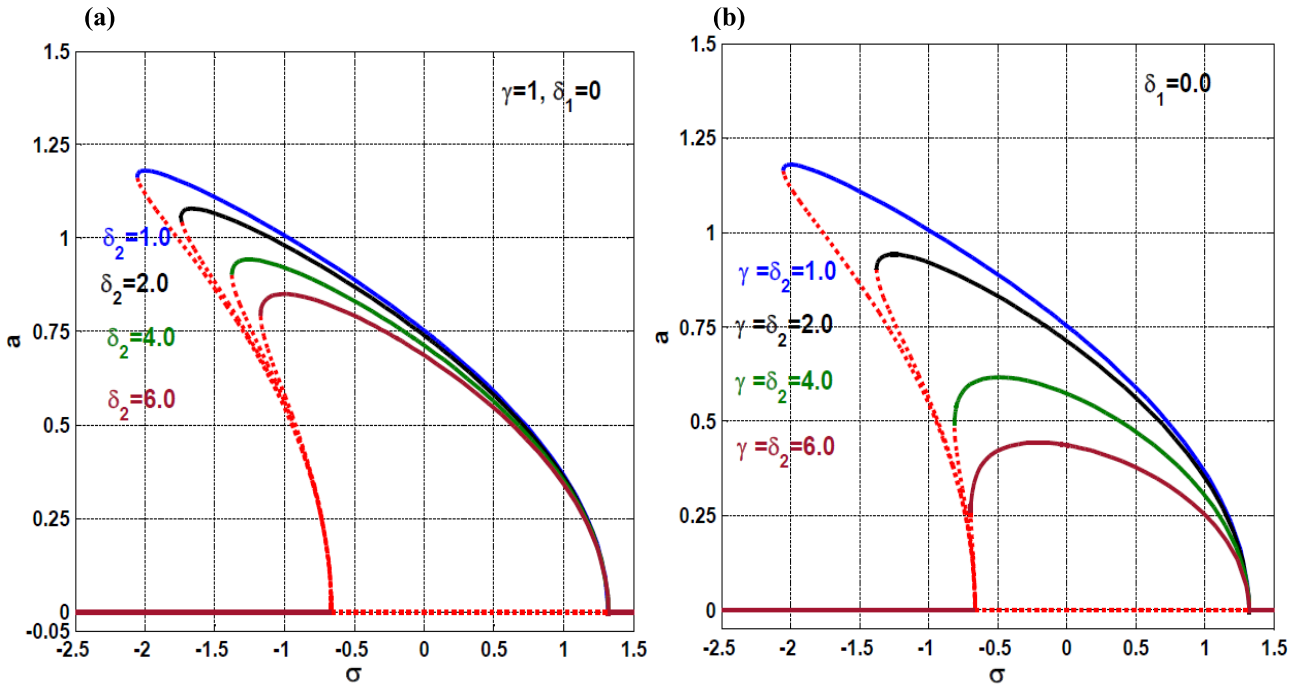

FIGURE 6. The controlled system frequency-response curves at different values of both the linear control gain and nonlinear feedback gain when $\delta_1 = 0.0$: (a) the system frequency-response curve at four different values of the nonlinear feedback gain δ_2 when $\gamma = 1.0$, and (b) the system frequency-response curve at four different values of both the control signal gain and nonlinear feedback gain.

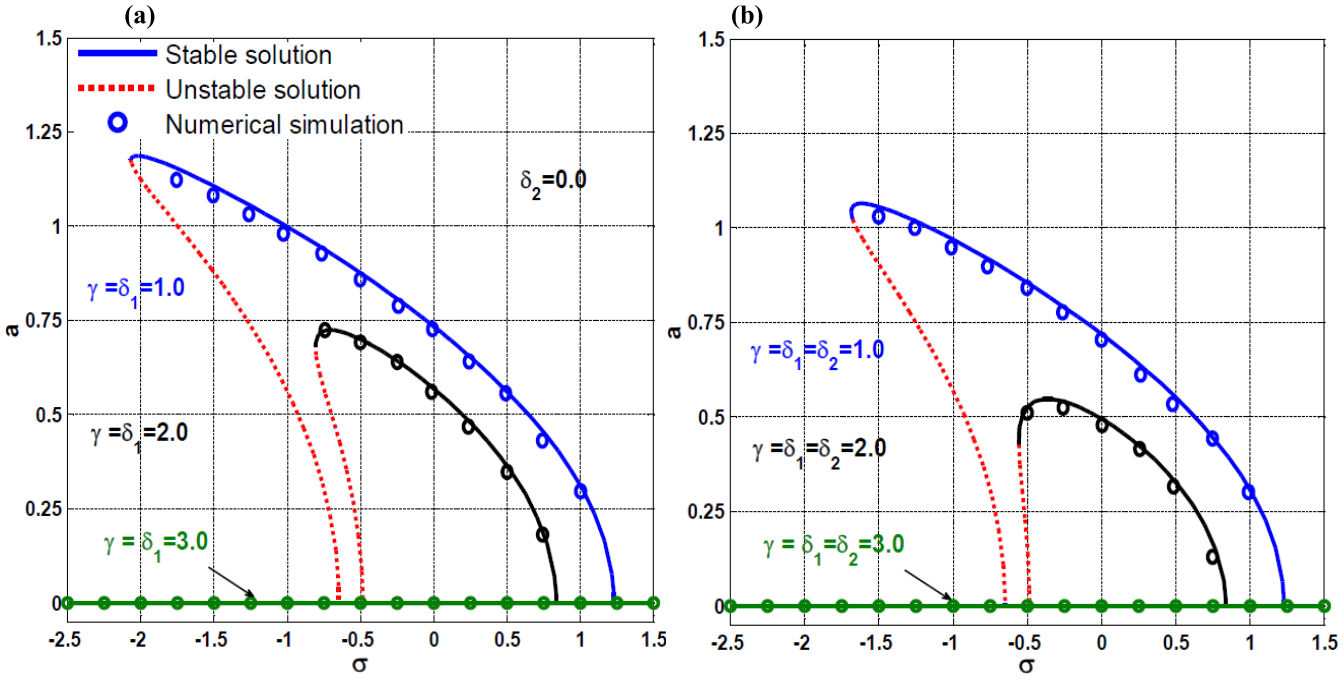

FIGURE 7. The controlled system frequency-response curves: (a) at three different values of both the control gain and linear feedback gain, and (b) at three different values of both the control gain, linear feedback gain, and nonlinear feedback gain.

the control and feedback gains are lower than three. (i.e., $\gamma = \delta_1 = \delta_2 < 3$).

Numerical simulations for the oscillatory behaviors of the considered system are illustrated in Fig. 8 according to Fig. 7 at $\sigma = 0.0$. Fig. 8a shows the system temporal oscillations according to Fig. 7awhen $\sigma = \delta_2 = 0.0$ for three different values of the linear control and feedback gains (i.e. $\gamma = \delta_1 = 1, 2, 3$), while Fig. 8b illustrates the system temporal oscillations according to Fig. 7b when $\sigma = 0.0$ for three different values of the control and feedback gains

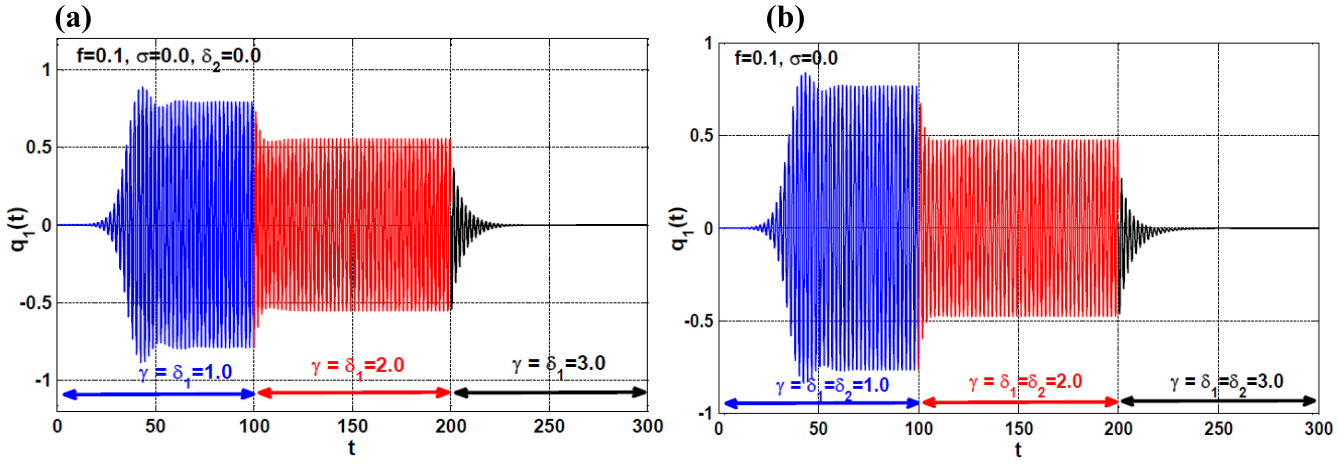

FIGURE 8. The time-history of the controlled system according to Fig. 7 when $\sigma = 0$: (a) the system time history according to Fig. 7a when sweeping the control gain (γ) and linear feedback gain (δ_1) from 1 to 2, then to 3 at $\delta_2 = 0.0$, and (b) the system time history according to Fig. 7b when sweeping the control gain (γ), linear feedback gain (δ_1), and nonlinear feedback gain (δ_2) from 1 to 2, then to 3.

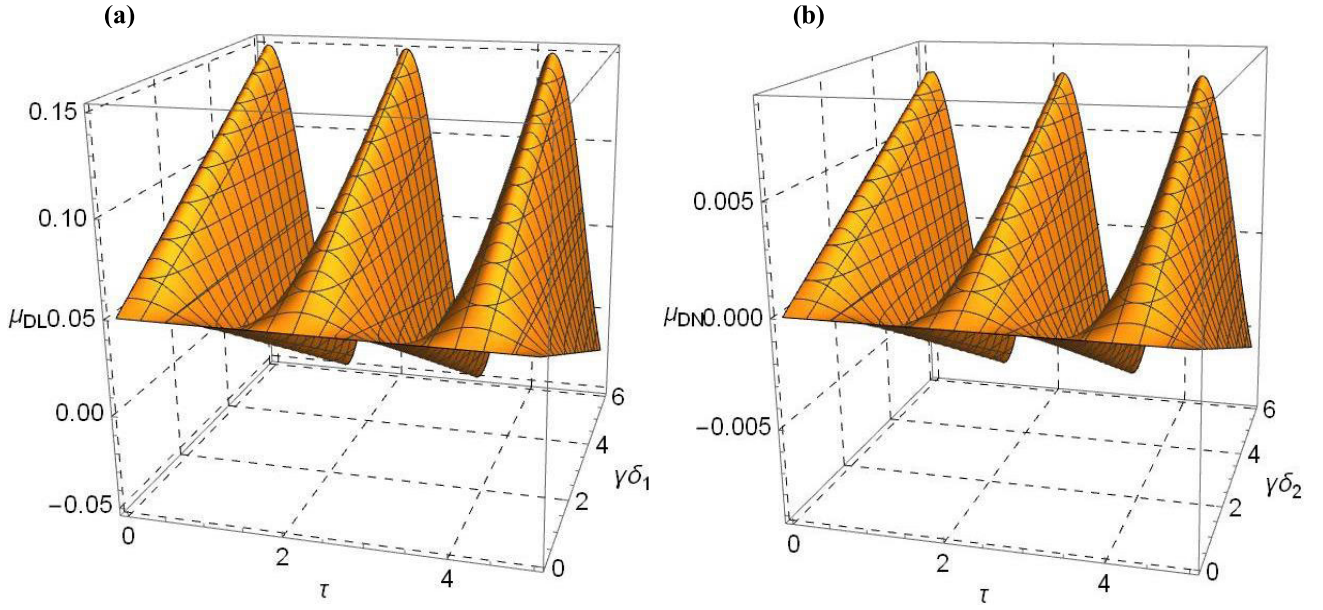

FIGURE 9. The controlled system equivalent damping coefficients μ_{DL} and μ_{DN} as a function of the time-delay ($\tau = \tau_1 + \tau_2$), the control gain γ and feedback gains δ_1 and δ_2: (a) the equivalent linear damping coefficient μ_{DL} as a function of the time-delay (τ) and the product of the linear control and feedback gains ($\gamma\delta_1$), and (b) the equivalent nonlinear damping coefficient μ_{DN} as a function of the time-delay (τ) and the product of the linear control gain and nonlinear feedback gain ($\gamma\delta_2$).

(i.e. $\gamma = \delta_1 = \delta_2 = 1, 2, 3$). It is clear from Fig. 8 that both the LIRC and the NIRC have suppressed the system oscillation amplitude to zero when $\gamma = \delta_1 = \delta_2 = 3$. However, the vibrations suppression efficiency of NIRC is higher than that of LIRC when $\gamma = \delta_1 = \delta_2 < 3$.

C. NONLINEAR INTEGRAL RESONANT CONTROLLER WITH TIME-DELAYS ($\tau = \tau_1 + \tau_2 \neq 0.0$)

The effect of the time-delays on the vibration mitigation performance of the introduced controller is discussed within this subsection depending on the obtained amplitude-phase modulating equations (i.e., Eqs. (22)). Referring to Eq. (22a), we can deduce that the linear and nonlinear damping coefficients of the time-delayed dynamical system given by Eqs. (2) can be expressed as follows:

$$\mu_{DL}(\tau, \gamma\delta_1) = \mu + \frac{\lambda\gamma\delta_1}{2\omega^2(\omega^2+\lambda^2)}\sin(\omega\tau) + \frac{\gamma\delta_1}{2\omega(\omega^2+\lambda^2)}\cos(\omega\tau) \quad (30.1)$$

$$\mu_{DN}(\tau, \gamma\delta_2) = \frac{3\lambda\gamma\delta_2}{8\omega^4(\omega^2+\lambda^2)}\sin(\omega\tau) + \frac{3\gamma\delta_2}{8\omega^3(\omega^2+\lambda^2)}\cos(\omega\tau) \quad (30.2)$$

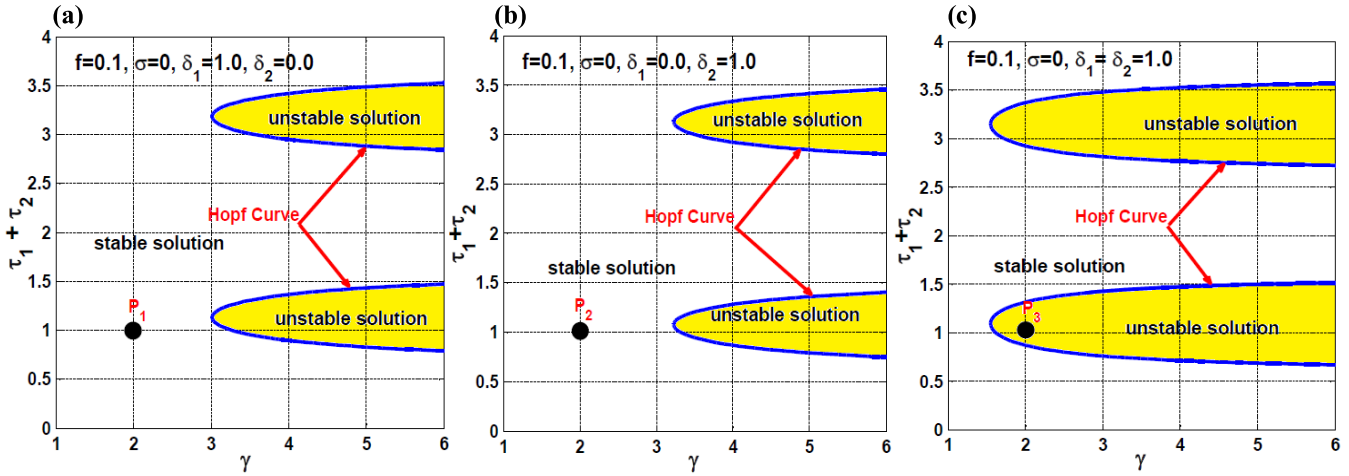

FIGURE 10. The controlled system stability charts in $\gamma - \tau$ plane at different values of the linear and nonlinear feedback signal gains when $f = \sigma = 0.0$: (a) the controlled system stability chart when $\delta_1 = 1.0$ and $\delta_2 = 0.0$, (b) the controlled system stability chart when $\delta_1 = 0.0$ and $\delta_2 = 1.0$, and (c) the controlled system stability chart when $\delta_1 = \delta_2 = 1.0$.

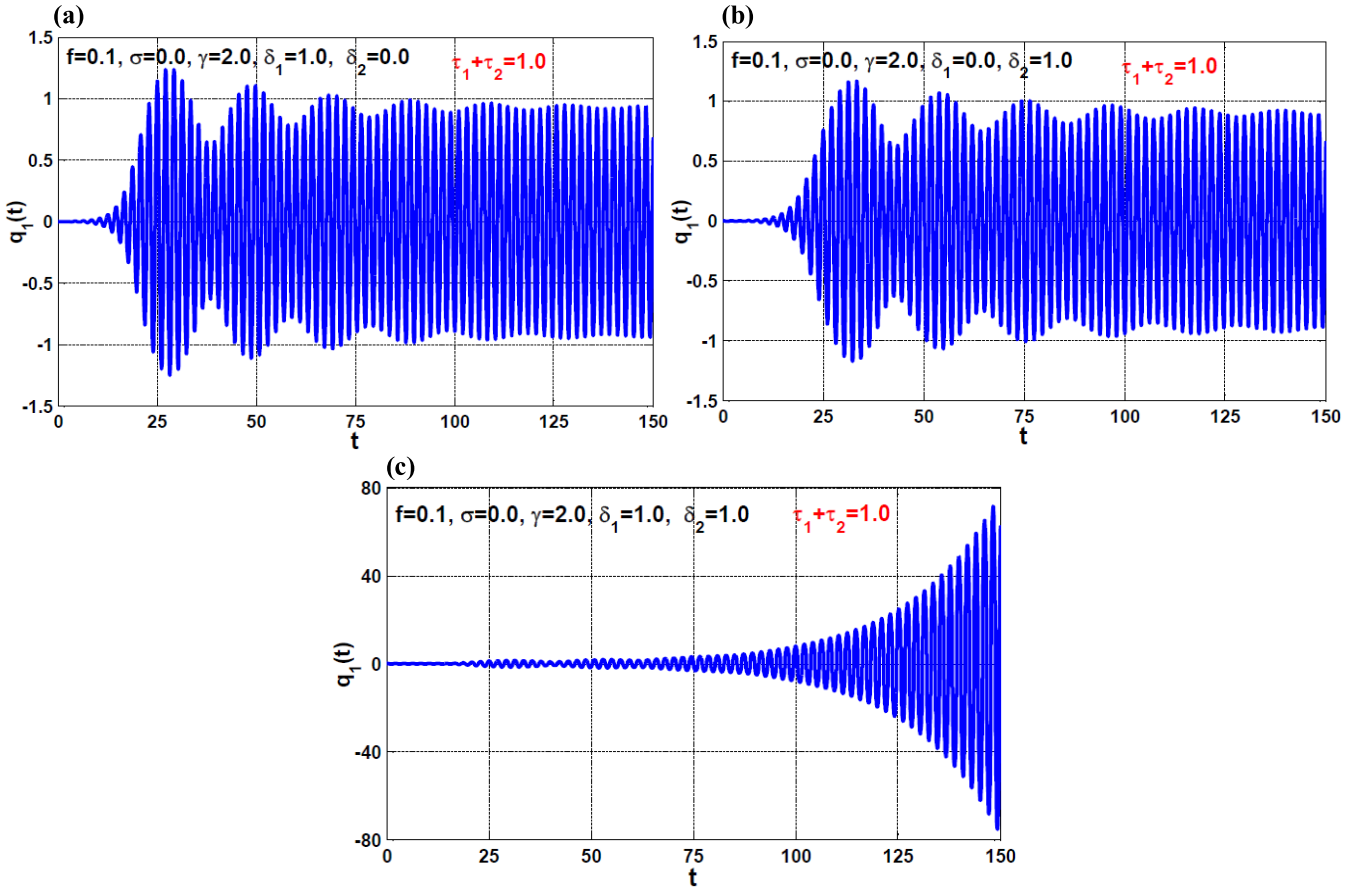

FIGURE 11. The controlled time-history according to Fig. 10: (a) the system time history according to the marked point P_1 on Fig. 10a (i.e., $f = 0.1, \sigma = 0, \delta_1 = 1.0, \delta_2 = 0.0, \gamma = 2, \tau_1 + \tau_2 = 1$), (b) the system time history according to the marked point P_2 on Fig. 10b (i.e. $f = 0.1, \sigma = 0, \delta_1 = 0.0, \delta_2 = 1.0, \gamma = 2, \tau_1 + \tau_2 = 1$), and (c) the system time history according to the marked point P_3 on Fig. 10c (i.e. $f = 0.1, \sigma = 0, \delta_1 = \delta_2 = 1.0, \gamma = 2, \tau_1 + \tau_2 = 1$).

where μ_{DL}, μ_{DN} are the linear and nonlinear damping coefficients of the time-delayed dynamical system, respectively, and $\tau = \tau_1 + \tau_2$. Referring to Eqs. (30), we can deduce that the linear damping coefficient (μ_{DL}) depends on the product of γ and δ_1 and on the sum of the loop delays (i.e. $\tau = \tau_1 + \tau_2$), while the nonlinear damping coefficient (μ_{DN}) depends on the product of γ and δ_2 and on the sum of the loop delays (i.e. $\tau = \tau_1 + \tau_2$). Accordingly, the two functions $\mu_{DL}(\tau, \gamma\delta_1)$

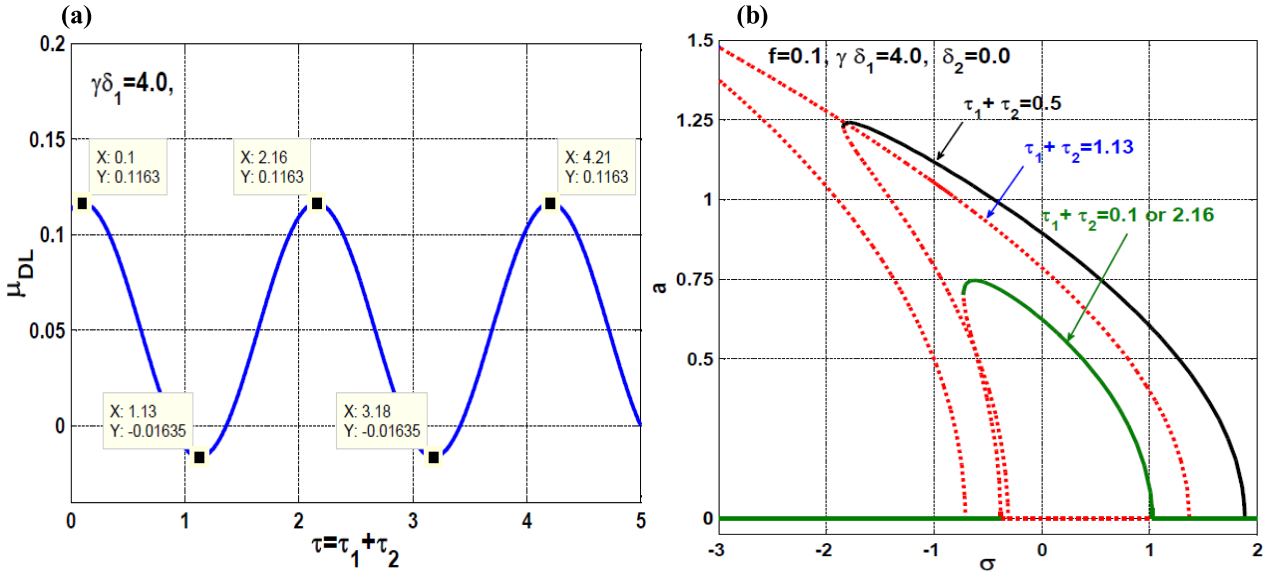

FIGURE 12. (a) the equivalent linear damping coefficient of the controlled system (μ_{DL}) versus the loop-delays ($\tau = \tau_1 + \tau_2$) when $\gamma\delta_1 = 4.0$, and (b) the controlled system frequency response-curve according to Fig. 12a at three different values of the loop-delay ($\tau_1 + \tau_2$).

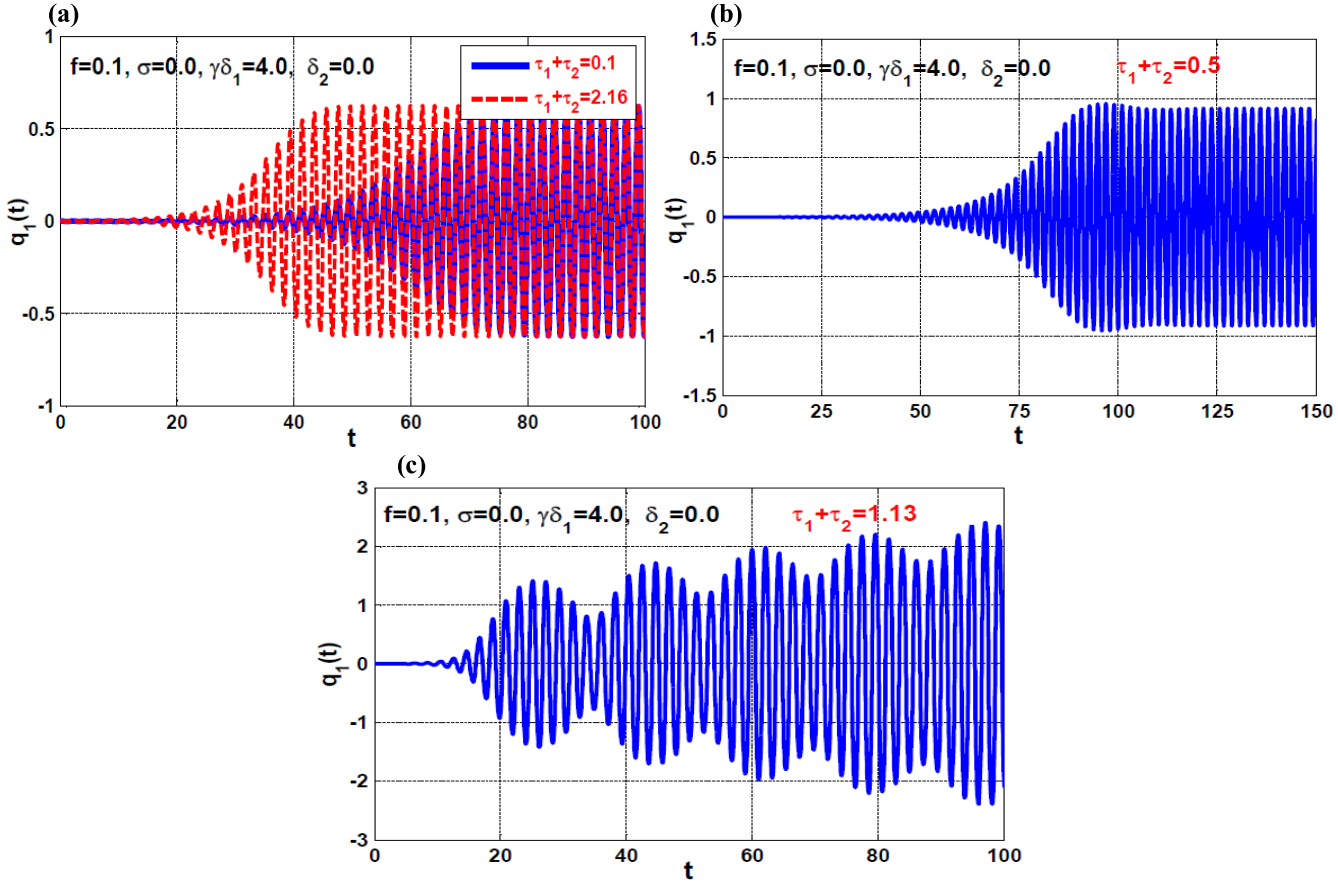

FIGURE 13. The controlled system time-history according to Fig. 12b: (a) the system time-history according to Fig. 12b when $\tau_1 + \tau_2 = 0.1$ and 2.16, (b) the system time-history according to Fig. 12b when $\tau_1 + \tau_2 = 0.5$, and (c) the system time-history according to Fig. 12b when $\tau_1 + \tau_2 = 1.13$.

and $\mu_{DN}(\tau, \gamma\delta_2)$ are plotted as a function of two variables in Fig. 9. It is clear from the figure that μ_{DL} and μ_{DN} are periodic functions of the sum of the loop delays. In addition, increasing the control gain (γ) and the feedback gains (δ_1 and δ_2) increases the fluctuation of the two functions making them fluctuate between the positive and negative

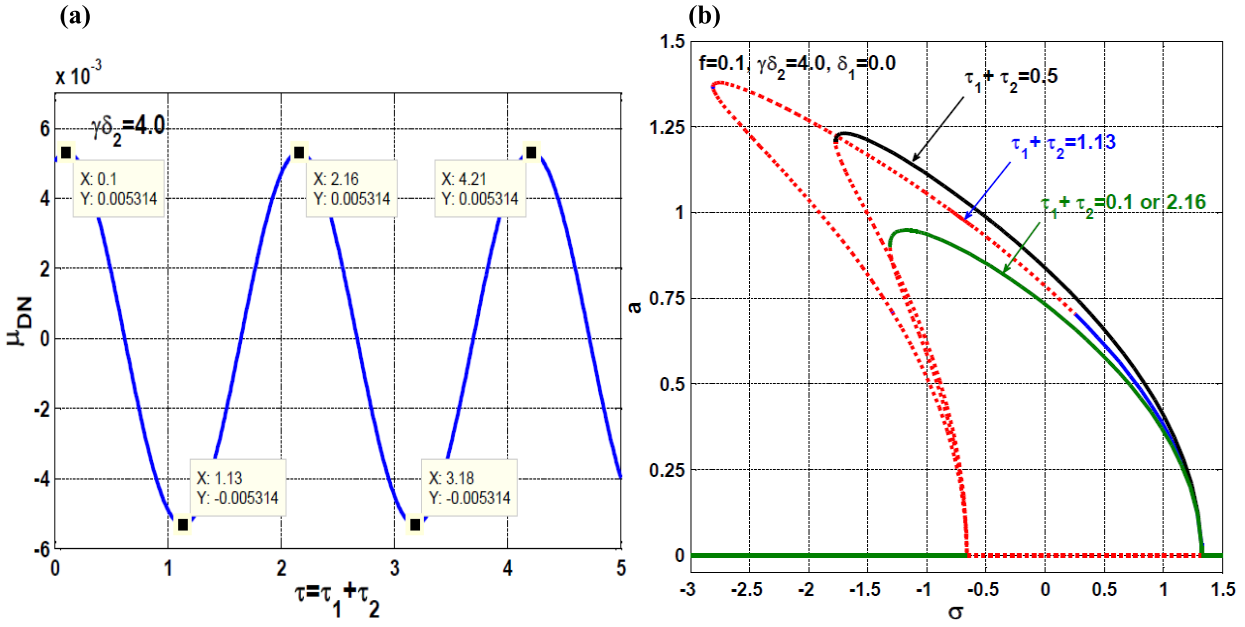

FIGURE 14. (a) The equivalent nonlinear damping coefficient of the controlled system (μ_{DN}) versus the loop-delay ($\tau = \tau_1 + \tau_2$) when $\gamma\delta_2 = 4.0$, $\delta_1 = 0.0$, and (b) the controlled system frequency response-curve according to Fig. 14a at three different values of the loop-delay ($\tau_1 + \tau_2$).

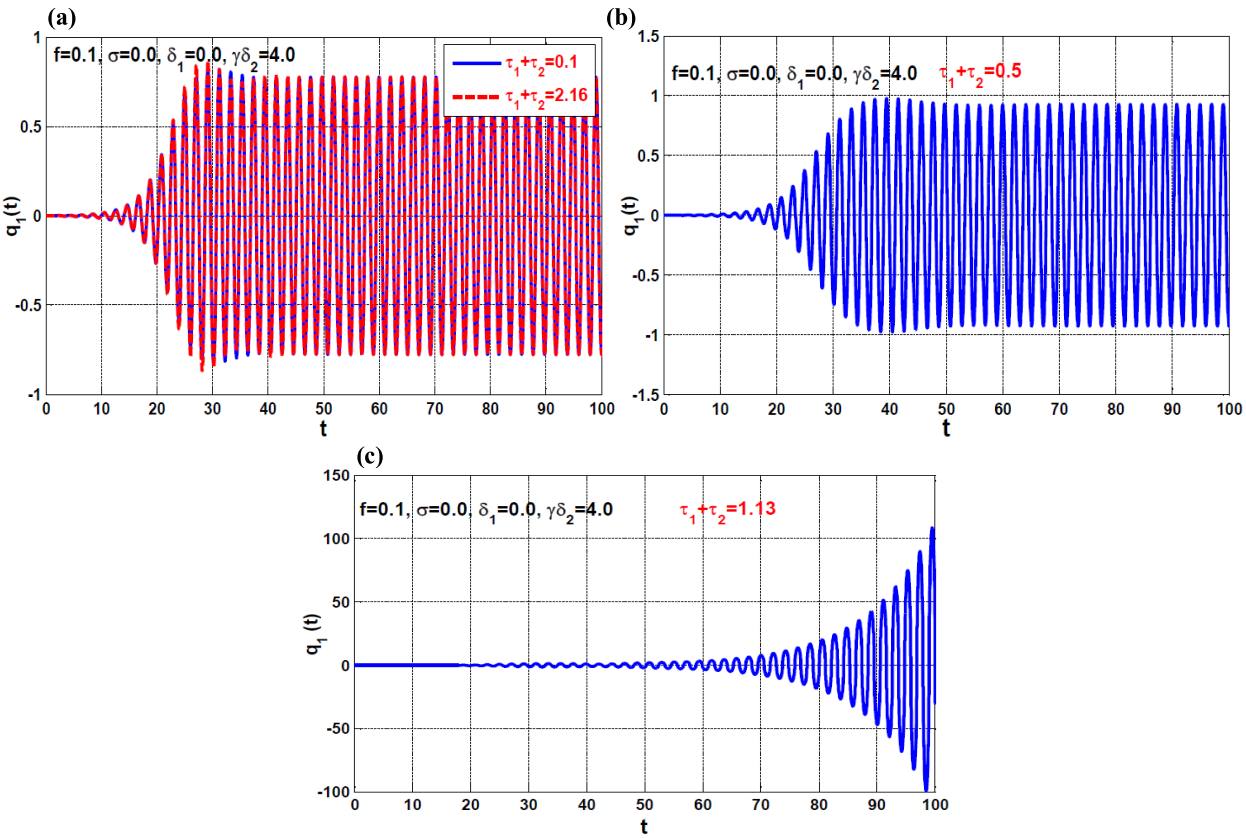

FIGURE 15. The controlled system time-history according to Fig. 14b: (a) the system time-history according to Fig. 14b when $\tau_1 + \tau_2 = 0.1$ and 2.16, (b) the system time-history according to Fig. 14b when $\tau_1 + \tau_2 = 0.5$, and (c) the system time-history according to Fig. 14b when $\tau_1 + \tau_2 = 1.13$.

values as is clear in Fig. 9. Accordingly, the existence of the time-delays in the control loop of the proposed controller (i.e., LIRC or NIRC) may improve the controller efficiency via selecting the loop-delays (τ) and the control parameters ($\gamma, \delta_1, \delta_2$) in such a way as to maximize $\mu_{DL}(\tau, \gamma\delta_1)$ and $\mu_{DN}(\tau, \gamma\delta_2)$. However, the time-delays may be the main

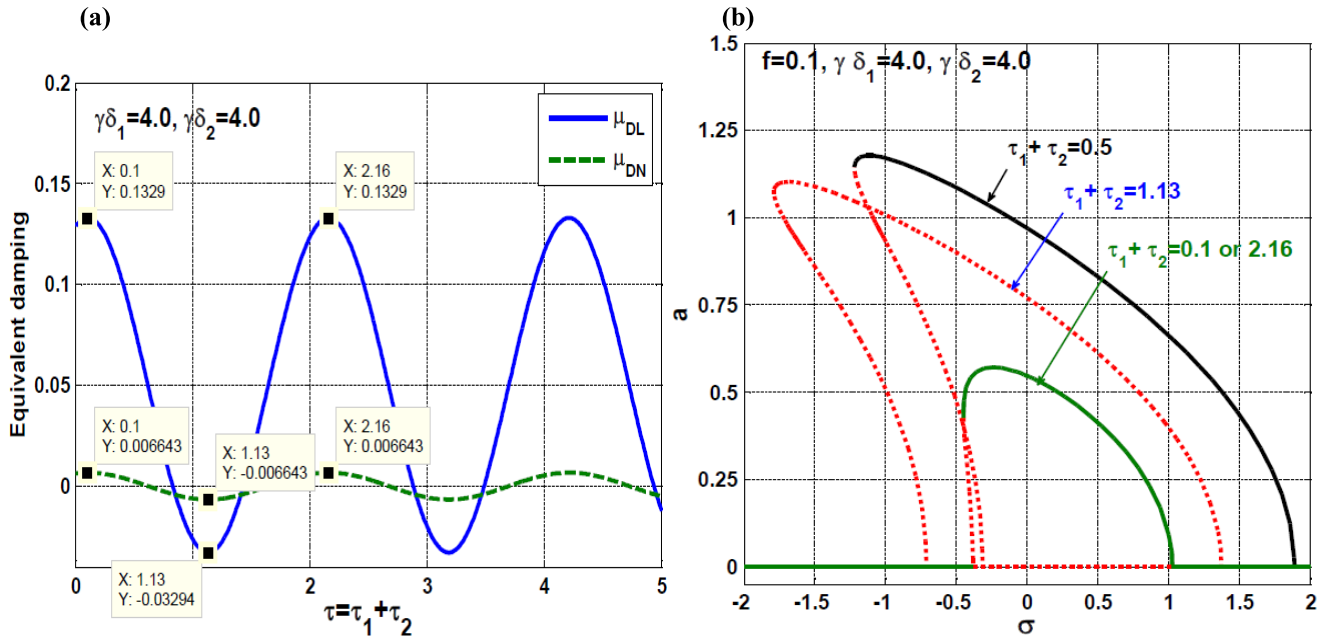

FIGURE 16. (a) The equivalent linear and nonlinear damping coefficients of the controlled system versus the loop-delay ($\tau = \tau_1 + \tau_2$) when $\gamma\delta_1 = \gamma\delta_2 = 4.0$, and (b) the controlled system frequency response-curve according to Fig. 16a at three different values of the loop-delay ($\tau_1 + \tau_2$).

reason for the system instability if the loop-delays and control parameters are selected in such a way that makes $\mu_{DL}(\tau, \gamma\delta_1) < 0$ and $\mu_{DN}(\tau, \gamma\delta_2) < 0$.

Accordingly, the stability chart of the considered system has been plotted depending on Eqs. (24, 26) as shown in Fig. 10 for different values of the feedback signal gains (δ_1 and δ_2). Fig. 10a shows the system stability chart in $\gamma - \tau$ plane when $f = 0.1, \sigma = 0.0, \delta_1 = 1.0, \delta_2 = 0$, Fig. 10b illustrates the system stability chart in $\gamma - \tau$ plane when $f = 0.1, \sigma = 0.0, \delta_1 = 0, \delta_2 = 1.0$, and Fig. 10c depicts the system stability chart in $\gamma - \tau$ plane when $f = 0.1$, $\sigma = 0.0, \delta_1 = \delta_2 = 1$. The unstable solution regions are illustrated as a yellow area surrounded by a Hopf-curve. By comparing Fig. 9 and Fig. 10, we can deduce that Fig. 10 is the projection of Fig. 9 on $\gamma - \tau$ plane, where the unstable solution regions in Fig.10 are the areas at which $\mu_{DL} < 0$ or/and $\mu_{DN} < 0$ as shown in Fig. 9. It is worth to mention that the Hopf-curve is the loci of the solution of Eq. (24) at which the eigenvalues of Eq. (26) are pure imaginary, (a detailed analysis for obtaining the Hopf curve can be found in Refs. [32], [33]).

To validate the accuracy of the obtained stability charts in Fig. 10, a numerical simulation for the considered system according to the three marked points P_1, P_2, and P_3 has been performed via solving the system original equations (i.e., Eqs. (2)) utilizing the **MATLAB DDE23** algorithm as shown in Fig. 11, where Figs. 11a and 11b show the system temporal oscillation according to the points P_1 and P_2 that are marked on Figs. 10a and 10b, respectively. In addition, Fig. 11c shows the system temporal oscillation according to the point P_3 that is marked on Fig. 10c. Comparing Fig. 11 with Fig. 10, we can deduce that the system responds with a bounded oscillation amplitude as in Figs. 11a and 11b because the points P_1 and P_2 have been selected within the stable solution region. On the other hand, the controlled system responds with an unbounded oscillation amplitude as in Fig. 11c because the point P_3 has been selected within the unstable solution region.

Depending on the above discussion, the influence of the loop-delays ($\tau = \tau_1 + \tau_2$) as a new controller parameter on the controlled system frequency-response curve will be discussed here. The equivalent linear damping coefficient μ_{DL} is plotted as a function of the loop-delays only as shown in Fig. 12a when $\gamma\delta_1 = 4.0$. It is clear from the figure that the linear damping coefficient μ_{DL} is a periodic function of loop-delays ($\tau_1 + \tau_2$) that fluctuate between the negative and positive values. Accordingly, we can deduce that the optimum loop-delays value that improves the proposed controller efficiency is that which maximizes the linear damping coefficient μ_{DL} (i.e., the optimum loop-delays are $\tau = 0.1, 2.16, 4.21, \ldots$). On the other hand, the worst loop-delays value is that which minimizes the linear damping coefficient μ_{DL}(i.e., the worst loop-delays are $\tau = 1.13, 3.18, \ldots$). According to Fig. 12a, the controlled system frequency-response curve is obtained at different values of the loop-delays when $f = 0.1, \delta_2 = 0.0, \gamma\delta_1 = 4.0$ as shown in Fig. 12b. By comparing Figs. 12a and 12b, the best controller efficiency has occurred at $\tau_1 + \tau_2 = 0.1$ or 2.16, while the worst control performance has happened at $\tau_1 + \tau_2 = 1.13$.

To confirm the accuracy of the obtained frequency-response curves given by Fig. 12b, the controlled system

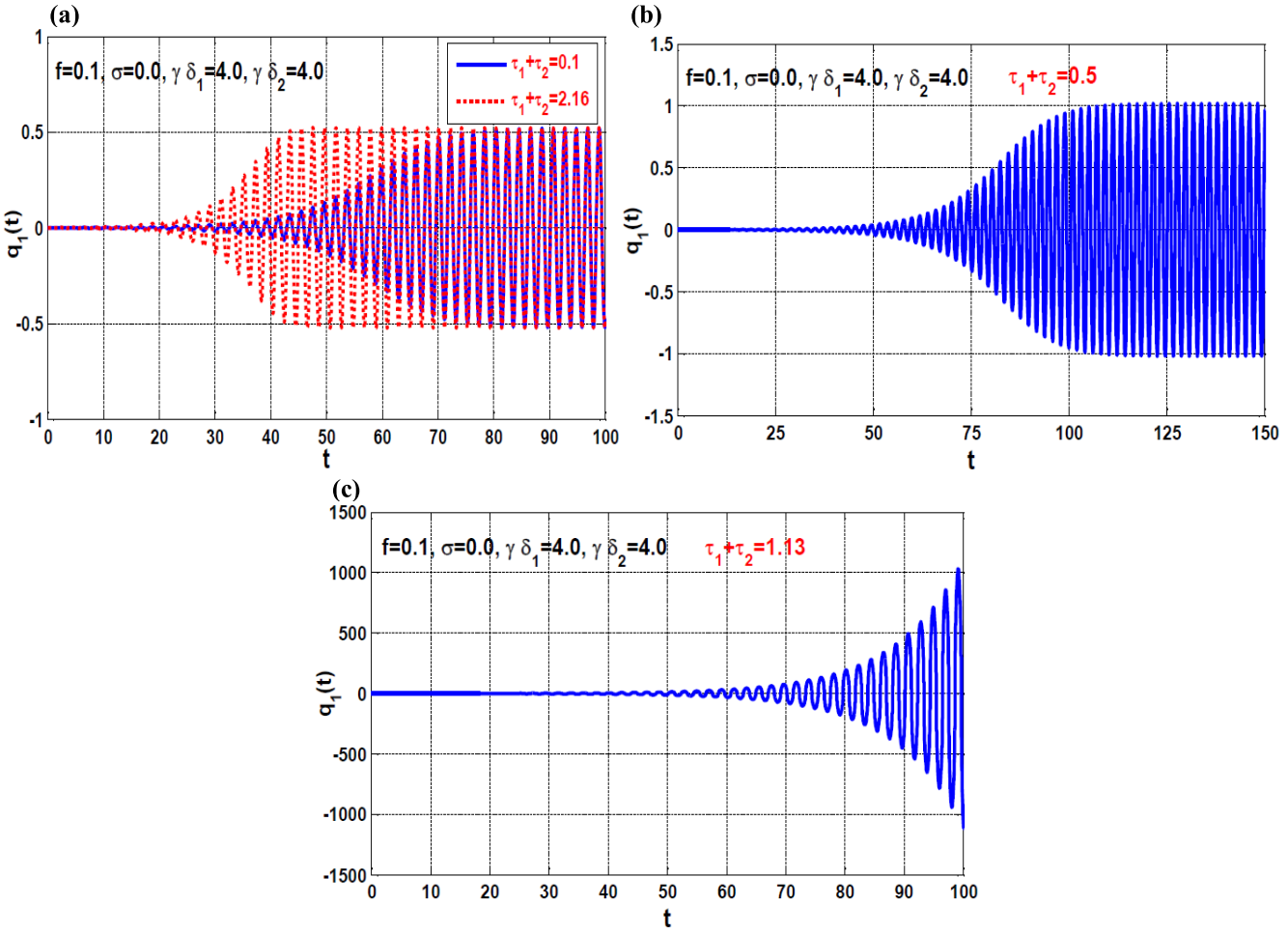

FIGURE 17. The controlled system time-history according to Fig. 16b: (a) the system time-history according to Fig. 16b when $\tau_1 + \tau_2 = 0.1$ and 2.16, (b) the system time-history according to Fig. 16b when $\tau_1 + \tau_2 = 0.5$, and (c) the system time-history according to Fig. 16b when $\tau_1 + \tau_2 = 1.13$.

temporal equations (i.e., Eqs. (2)) are numerically simulated according to Fig. 12b (i.e. when $f = 0.1, \gamma\delta_1 = 4.0, \delta_2 = 0.0, \sigma = 0.0$) for the different values of the loop-delays as shown in Fig. 13, where Fig. 13a illustrates the system time history according to Fig. 12b when $\sigma = 0.0$ at $\tau_1 + \tau_2 = 0.1$ and 2.16. In addition, Figs. 13b and 13c illustrate the system temporal oscillation according to Fig. 12b at $\sigma = 0.0$ when $\tau_1 + \tau_2 = 0.5$ and 1.13, respectively. According to Fig. 12a, 12b, and 13, we can confirm that the selection of the control parameters γ, δ_1, and $\tau_1 + \tau_2$ in such a way that maximizes μ_{DL} will optimize the control performance of the linear integral resonant controller.

The equivalent nonlinear damping coefficient μ_{DN} is plotted as a function of the loop-delays only as shown in Fig. 14a when $\gamma\delta_2 = 4.0$. It is clear from the figure that the nonlinear damping coefficient μ_{DN} is a periodic function of loop-delays $(\tau_1 + \tau_2)$ that fluctuate between the negative and positive values. Accordingly, we can deduce that the optimum loop-delays value that improves the proposed controller efficiency is that which maximizes the nonlinear damping coefficient μ_{DN} (i.e., the optimum loop-delays are $= 0.1, 2.16, 4.21, \ldots$). On the other hand, the worst loop-delays value is that which minimizes the nonlinear damping coefficient μ_{DN} (i.e., the worst loop-delays are $\tau = 1.13, 3.18, \ldots$). According to Fig. 14a, the controlled system frequency-response curve is obtained at different values of the loop-delays when $f = 0.1, \delta_1 = 0.0, \gamma\delta_2 = 4.0$ as shown in Fig. 14b. By comparing Figs. 14a and 14b, it is clear that the best controller efficiency has occurred at $\tau_1+\tau_2 = 0.1$ or 2.16, while the worst control performance has happened at $\tau_1 + \tau_2 = 1.13$.

To confirm the accuracy of the obtained frequency-response curves given by Fig. 14b, the controlled system temporal equations (i.e., Eqs. (2)) are numerically simulated according to Fig. 14b (i.e. when $f = 0.1, \gamma\delta_2 = 4.0, \delta_1 = 0.0$, and $\sigma = 0.0$) for the different values of the loop-delays as shown in Fig. 15, where Fig. 15a illustrates the system temporal oscillation according to Fig. 14b when $\sigma = 0.0$ at $\tau_1 + \tau_2 = 0.1$ and 2.16. Also, Figs. 15b and 15c illustrate the system temporal oscillation according to Fig. 14b when $\sigma = 0.0$ at $\tau_1 + \tau_2 = 0.5$ and 1.13, respectively. According to Fig. 14a, 14b, and 15, we can confirm that the selection of

the control parameters γ, δ_2, and $\tau_1 + \tau_2$ in such a way that maximizes μ_{DN} will optimize the control performance of the proposed controller.

The dynamical behaviors of the whole proposed controller (i.e., $\gamma \neq 0, \delta_1 \neq 0, \delta_2 \neq 0, \tau_1 + \tau_2 \neq 0$) are investigated as shown in Figs. 16 and 17. The equivalent linear and nonlinear damping coefficients are plotted as a function of the loop-delays only as shown in Fig. 16a when $\gamma\delta_1 = \gamma\delta_2 = 4.0$. It is clear from the figure the optimum loop-delays value that improves the controller efficiency is that which maximizes the linear and nonlinear damping coefficients. According to Fig. 16a, the controlled system frequency-response curve is obtained at different values of the loop-delays when $f = 0.1, \gamma\delta_1 = \gamma\delta_2 = 4.0$ as shown in Fig. 16b. By comparing Figs. 16a and 16b, it is clear that the best controller efficiency has occurred at $\tau_1 + \tau_2 = 0.1$ or 2.16, while the worst control performance has happened at $\tau_1 + \tau_2 = 1.13$. To confirm the accuracy of the obtained frequency-response curves given by Fig. 16b, the controlled system original equations (i.e., Eqs. (2)) are numerically simulated according to Fig. 16b (i.e. when $f = 0.1, \gamma\delta_1 = \gamma\delta_2 = 4.0$, and $\sigma = 0.0$) for the different values of the loop-delays as shown in Fig. 17, where Fig. 17a illustrates the system temporal oscillation according to Fig. 16b when $\sigma = 0.0$ at $\tau_1 + \tau_2 = 0.1$ and 2.16. Also, Figs. 17b and 17c illustrate the system temporal oscillation according to Fig. 16b when $\sigma = 0.0$ at $\tau_1 + \tau_2 = 0.5$ and 1.13, respectively. According to Fig. 16, and 17, we can confirm that the selection of the control parameters γ, δ_1, δ_2, and $\tau_1 + \tau_2$ in such a way that maximizes μ_{DL} and μ_{DN} will optimize the control performance of the proposed controller.

IV. CONCLUSION

The time-delayed nonlinear integral resonant controller is introduced to control the nonlinear oscillation of a parametrically excited system as a new control method. The controlled system is described by a time-delayed second-order nonlinear differential equation excited parametrically (i.e., beam system) and coupled to a first-order differential equation (i.e., controller). The multiple scales homotopy approach is applied to analyze the mathematical model of the controlled system. The influences of the different control parameters and the loop-delays on system steady-state vibration amplitude are explored via plotting the different bifurcation diagrams. Stability charts of the loop delays are obtained. The optimum working conditions for the proposed controller are reported either when the loop-delays are considered or neglected. Based on the obtained results, the following points can be concluded.

A. THE CONTROLLED SYSTEM WITHOUT TIME-DELAYS

1. The nonlinear integral resonant controller has modified the linear damping coefficient of the considered system (i.e., μ) to become $\mu_L = \mu + \frac{\gamma\delta_1}{2\omega(\omega^2+\lambda^2)}$. In addition, the nonlinear damping coefficient $\mu_N = \frac{3\gamma\delta_2}{8\omega^3(\omega^2+\lambda^2)}$ has appeared in the amplitude-phase modulating equations.
2. The efficiency of the linear integral resonant controller (i.e., when $\delta_2 = 0.0$) depends on the product of the linear feedback gain (δ_1) and control gain (γ).
3. The efficiency of the nonlinear integral resonant controller depends on the product of the linear feedback gain (δ_1) and control gain (γ) as well as the product of the nonlinear feedback gain (δ_2) and control gain (γ).
4. The selection of the control and feedback signal gains in such a way that maximizes ($\gamma \times \delta_1$) and ($\gamma \times \delta_2$) will improve the proposed controller efficiency in suppressing the system parametric vibrations.

B. THE CONTROLLED SYSTEM WITH TIME-DELAYS

5. The time-delayed nonlinear integral resonant controller has modified the linear damping coefficient of the considered system (i.e. μ) to become $\mu_{DL} = \mu + \frac{\lambda\gamma\delta_1}{2\omega^2(\omega^2+\lambda^2)}\sin(\omega\tau) + \frac{\gamma\delta_1}{2\omega(\omega^2+\lambda^2)}\cos(\omega\tau)$ and the nonlinear damping coefficient became $\mu_{DN} = \frac{3\lambda\gamma\delta_2}{8\omega^4(\omega^2+\lambda^2)}\sin(\omega\tau) + \frac{3\gamma\delta_2}{8\omega^3(\omega^2+\lambda^2)}\cos(\omega\tau)$, where τ is the sum of the time-delays in the control loop (i.e. $\tau = \tau_1 + \tau_2$).
6. Depending on point (5), the controlled system damping coefficients (μ_{DL} and μ_{DN}) are periodic functions of the sum of the loop-delays, where μ_{DL} and μ_{DN} can fluctuate between the positive and negative values depending on the magnitude of both the control and feedback signal gains.
7. Selecting the loop-delays in such a way that maximizes the linear and nonlinear damping coefficients (μ_{DL} and μ_{DN}) will optimize the vibration suppression efficiency of the proposed controller.
8. Selecting the loop-delays in such a way that minimizes the linear and nonlinear damping coefficients (μ_{DL} and μ_{DN}) will be destabilized the controlled system as in Figs. 13c, 15c, and 17c.
9. The nonlinear integral resonant controller is more efficient than the linear integral resonant controller, where the nonlinear one adds nonlinear damping to the controlled system besides increasing its linear damping coefficient.
10. Finally, it is recommended to implement the time-delayed nonlinear integral resonant controller experimentally in the future as an efficient control strategy in suppressing the parametrically excited oscillations.

ACKNOWLEDGMENT

The authors would like to thank the Taif University. This work was supported by the Taif University Researchers Supporting Project, Taif University, Taif, Saudi Arabia, under Grant TURSP-2020/160.

REFERENCES

[1] S. S. Oueini and H. A. Nayfeh, "Single-mode control of a cantilever beam under principal parametric excitation," *J. Sound Vib.*, vol. 224, no. 1, pp. 33–47, Jul. 1999.

[2] H. Yabuno, T. Murakami, J. Kawazoe, and N. Aoshima, "Suppression of parametric resonance in cantilever beam with a pendulum (Effect of static friction at the supporting point of the pendulum)," *J. Vib. Acoust.*, vol. 126, no. 1, pp. 149–162, Jan. 2004.

[3] L. Chen, F. He, and K. Sammut, "Vibration suppression of a principal parametric resonance," *J. Vib. Control*, vol. 15, no. 3, pp. 439–463, Mar. 2009.

[4] B. Pratiher, "Vibration control of a transversely excited cantilever beam with tip mass," *Arch. Appl. Mech.*, vol. 82, no. 1, pp. 31–42, Jan. 2012.

[5] A. Maccari, "Vibration control for the primary resonance of a cantilever beam by a time delay state feedback," *J. Sound Vib.*, vol. 259, no. 2, pp. 241–251, Jan. 2003.

[6] K. A. Alhazza, A. H. Nayfeh, and M. F. Daqaq, "On utilizing delayed feedback for active-multimode vibration control of cantilever beams," *J. Sound Vib.*, vol. 319, nos. 3–5, pp. 735–752, Jan. 2009.

[7] K. A. Alhazza and M. A. Majeed, "Free vibrations control of a cantilever beam using combined time delay feedback," *J. Vib. Control*, vol. 18, no. 5, pp. 609–621, Apr. 2012.

[8] M. F. Daqaq, K. A. Alhazza, and Y. Qaroush, "On primary resonances of weakly nonlinear delay systems with cubic nonlinearities," *Nonlinear Dyn.*, vol. 64, no. 3, pp. 253–277, May 2011.

[9] J. Peng, G. Zhang, M. Xiang, H. Sun, X. Wang, and X. Xie, "Vibration control for the nonlinear resonant response of a piezoelectric elastic beam via time-delayed feedback," *Smart Mater. Struct.*, vol. 28, no. 9, Sep. 2019, Art. no. 095010.

[10] N. A. Saeed and W. A. El-Ganaini, "Utilizing time-delays to quench the nonlinear vibrations of a two-degree-of-freedom system," *Meccanica*, vol. 52, nos. 11–12, pp. 2969–2990, Sep. 2017.

[11] N. A. Saeed and W. A. El-Ganaini, "Time-delayed control to suppress the nonlinear vibrations of a horizontally suspended jeffcott-rotor system," *Appl. Math. Model.*, vol. 44, pp. 523–539, Apr. 2017.

[12] N. A. Saeed, G. M. Moatimid, F. M. F. Elsabaa, and Y. Y. Ellabban, "Time-delayed control to suppress a nonlinear system vibration utilizing the multiple scales homotopy approach," *Arch. Appl. Mech.*, vol. 91, no. 3, pp. 1193–1215, Mar. 2021.

[13] N. A. Saeed, G. M. Moatimid, F. M. Elsabaa, Y. Y. Ellabban, M. A. El-Meligy, and M. Sharaf, "Time-delayed nonlinear feedback controllers to suppress the principal parameter excitation," *IEEE Access*, vol. 8, pp. 226151–226166, 2020.

[14] J. Xu, K. W. Chung, and Y. Y. Zhao, "Delayed saturation controller for vibration suppression in a stainless-steel beam," *Nonlinear Dyn.*, vol. 62, nos. 1–2, pp. 177–193, Oct. 2010.

[15] N. A. Saeed, W. A. El-Ganini, and M. Eissa, "Nonlinear time delay saturation-based controller for suppression of nonlinear beam vibrations," *Appl. Math. Model.*, vol. 37, nos. 20–21, pp. 8846–8864, Nov. 2013.

[16] N. A. Saeed and H. A. El-Gohary, "Influences of time-delays on the performance of a controller based on the saturation phenomenon," *Eur. J. Mech. A, Solids*, vol. 66, pp. 125–142, Nov. 2017.

[17] M. Eissa, M. Kamel, N. A. Saeed, W. A. El-Ganaini, and H. A. El-Gohary, "Time-delayed positive-position and velocity feedback controller to suppress the lateral vibrations in nonlinear Jeffcott-rotor system," *Menoufia J. Electron. Eng. Res.*, vol. 27, no. 1, pp. 261–278, 2018.

[18] X. Sun and J. Xu, "Vibration control of nonlinear absorber–isolator-combined structure with time-delayed coupling," *Int. J. Non-Linear Mech.*, vol. 83, pp. 48–58, Jul. 2016.

[19] X. Sun, S. Zhang, and J. Xu, "Parameter design of a multi-delayed isolator with asymmetrical nonlinearity," *Int. J. Mech. Sci.*, vols. 138–139, pp. 398–408, Apr. 2018.

[20] X. Sun, F. Wang, and J. Xu, "Dynamics and realization of a feedback-controlled nonlinear isolator with variable time delay," *J. Vib. Acoust.*, vol. 141, no. 2, Art. no. 0210052, 2019, doi: 10.1115/1.4041369.

[21] I. M. Díaz, E. Pereira, and P. Reynolds, "Integral resonant control scheme for cancelling human-induced vibrations in light-weight pedestrian structures," *Struct. Control Health Monitor.*, vol. 19, no. 1, pp. 55–69, Feb. 2012.

[22] A. Al-Mamun, E. Keikha, C. S. Bhatia, and T. H. Lee, "Integral resonant control for suppression of resonance in piezoelectric micro-actuator used in precision servomechanism," *Mechatronics*, vol. 23, no. 1, pp. 1–9, Feb. 2013.

[23] E. Omidi and S. N. Mahmoodi, "Sensitivity analysis of the nonlinear integral positive position feedback and integral resonant controllers on vibration suppression of nonlinear oscillatory systems," *Commun. Nonlinear Sci. Numer. Simul.*, vol. 22, nos. 1–3, pp. 149–166, May 2015.

[24] E. Omidi and S. N. Mahmoodi, "Nonlinear vibration suppression of flexible structures using nonlinear modified positive position feedback approach," *Nonlinear Dyn.*, vol. 79, no. 2, pp. 835–849, Jan. 2015.

[25] E. Omidi and S. N. Mahmoodi, "Nonlinear integral resonant controller for vibration reduction in nonlinear systems," *Acta Mechanica Sinica*, vol. 32, no. 5, pp. 925–934, Oct. 2016.

[26] J. D. J. MacLean and S. S. Aphale, "A modified linear integral resonant controller for suppressing jump-phenomenon and hysteresis in micro-cantilever beam structures," *J. Sound Vib.*, vol. 480, Aug. 2020, Art. no. 115365.

[27] A. Mitura, J. Warminski, and M. Bochenski, "Optimal control methods for vertical and horizontal beam dynamics," *J. Phys. Conf.*, vol. 382, Aug. 2012, Art. no. 012041, doi: 10.1088/1742-6596/382/1/012041.

[28] Y. O. El-Dib, "Stability analysis of a strongly displacement time-delayed Duffing oscillator using multiple scales homotopy perturbation method," *J. Appl. Comput. Mech.*, vol. 4, no. 4, pp. 260–274, 2018.

[29] G. M. Moatimid, F. M. F. Elsabaa, and M. H. Zekry, "Approximate solutions of coupled nonlinear oscillations: Stability analysis," *J. Appl. Comput. Mech.*, vol. 6, no. SI, pp. 1404–1417, 2020.

[30] A. Nayfeh and D. Mook, *Nonlinear Oscillations*. New York, NY, USA: Wiley, 1979.

[31] W. A. El-Ganaini, N. A. Saeed, and M. Eissa, "Positive position feedback (PPF) controller for suppression of nonlinear system vibration," *Nonlinear Dyn.*, vol. 72, no. 3, pp. 517–537, May 2013.

[32] W. Govaerts, Y. A. Kuznetsov, and B. Sijnave, "Implementation of Hopf and double-Hopf continuation using bordering methods," *ACM Trans. Math. Softw.*, vol. 24, no. 4, pp. 418–436, 1998.

[33] W. Govaerts, *Numerical Methods for Bifurcations of Dynamical Equilibria*. Philadelphia, PA, USA: SIAM, 2000.

N. A. SAEED was born in Menoufia, Egypt, in 1986. He received the B.Sc. degree in industrial electronics and control engineering from the Department of Industrial Electronics and Control Systems, Faculty of Electronic Engineering, Menoufia University, Egypt, in 2008, and the M.Sc. and Ph.D. degrees in engineering mathematics from the Department of Physics and Engineering Mathematics, Faculty of Electronic Engineering, Menoufia University, in 2014 and 2018, respectively. Since 2018, he has been an Assistant Professor with the Department of Physics and Engineering Mathematics, Faculty of Electronic Engineering, Menoufia University. He is the author of more than 35 articles published in high reputable journals. He developed his researches in the field of nonlinear dynamics, bifurcation theory, linear and nonlinear vibrations control, perturbation methods, time-delayed systems, rotor-dynamics, and rotor active magnetic bearings systems.

GALAL M. MOATIMID was born in El-Sharkia, Egypt, in 1954. He received the B.Sc. and M.Sc. degrees in mathematics from Ain Shams University, Egypt, in 1980 and 1984, respectively, and the Ph.D. degree from Tanta University, Egypt, in 1990. He was an Associate Professor and a Full Professor, in 1995 and 2004, respectively. His previous work is concerned with electrohydrodynamics stability. He is an author and co-workers of more than 120 research articles, all of them are published in highly specialized international journals. His current research is disturbed with different perturbation techniques.

FAWZY M. ELSABAA was born in Port Said, Egypt, in 1946. He received the B.Sc. degree in mathematics from Ain Shams University, Cairo, Egypt, in 1970, and the Ph.D. degree in applied mathematics from Moscow State University, in 1979. Since 1997, he has been a Full Professor with the Faculty of Education, Ain Shams University. His current research interests include nonlinear dynamics, celestial mechanics, galaxy motion, and mechanics of rigid bodies.

YOMNA Y. ELLABBAN was born in Cairo, Egypt, in 1993. She received the B.S. degree in science and education in mathematics from the Faculty of Education, Ain Shams University, Egypt, in 2015, and the General Diploma degree in pure and applied mathematics and Special Diploma degree in applied mathematics from the Department of Mathematics, Faculty of Education, Ain Shams University, in 2016 and 2017, respectively. She is currently pursuing the preliminary M.A. degree. Her current research interests include time-delayed systems, linear and nonlinear vibration control, nonlinear dynamics, and perturbation methods.

S. K. ELAGAN received the M.Sc. and Ph.D. degrees from the Department of Mathematics and Computer Sciences, Faculty of Science, Menofiya University, in 2008. He is currently an Assistant Professor with the Department of Mathematics and Statistics, Faculty of Science, Taif University, Saudi Arabia. His main research interests include semigroup theory, fractional differential equations, DNA modeling, and algebraic topology.

MOHAMED S. MOHAMED received the M.Sc. and Ph.D. degrees in mathematics from the Faculty of Science, Al-Azhar University, Cairo, Egypt, in 2002 and 2007, respectively. He is currently a Full Professor of mathematics with the Department of Mathematics, Faculty of Science, Al-Azhar University. He is the author of more than 70 scientific articles and two textbooks in refereed journals and international conferences. His research interests include theory of differential equations and its application, numerical analysis, modeling, numerical and semi-analytical, and computational methods for solving differential equations. He has supervised and examined some of the M.Sc. and Ph.D. degrees students.